23 December 2025

Where air-conditioning is essential: Raising a yellow flag ten times - where wet bulb globe temperature under shaded outdoor shelter fails to refresh adapted healthy individuals

Eric Laurentius Peterson, University of Leeds (email contact **e.peterson@leeds.ac.uk**)

Abstract

Concerning the modern paradigm shift to insulate building envelopes with the ambition to improve winter comfort without demand for heating, unintended problems can arise in summer as insulation traps heat and humidity from cooking and occupants' respiration. So, we should consider outdoor living areas, covered from sun and rain, but openly alfresco - such as verandas. The current work extends on a counterfactual approach to designing air-conditioning that considered passive and low energy alternatives. That research found air-conditioning is desirable on days when conditions exceed 25.6°C daily maximum wet-bulb globe temperature in shade (WBGTs) – referred to as a "white-flag" day (Wsd). Furthermore, access to cool shelter becomes a necessity for a greater proportion of the population if maximum outdoor WBGTs exceeds 29.4°C – referred to as a "yellow-flag" day (Ysd). Global mapping highlights practical limits of passive and low energy alternatives to air-conditioning, but lack of weather stations overlook urban heat islands. Accepting that there may be poorly designed dwellings prone to dangerous overheating that demands active cooling while neighbouring parks and gardens may provide passively cool relief – the current work broadly identifies observed and forecasted limits of shaded outdoor living areas as an effective refuge. Analysis of weather stations' annals (1987-2020) of threshold-days are globally mapped, classified by annual exceedance. Standard deviations of interannual variability are added to long term averages, compared with standard estimate of error added to linear regression intercept at the last year –

to estimate days white- and yellow-flag conditions in shade were exceeded in hotter years (WsD† and YsD†). Finding where WsD† exceed 10 days per "hot" year but Ysd had not, thence these 4661 locations are now reanalysed with respect to accessible observations during the 50 years through 2024 and projected to 2050. The number of locations exceeding thresholds generally increased, while local exceptions are detailed in supporting material. Air-conditioned shelters are needed by more vulnerable people, while passive and low energy solutions should be delivered whenever practical so that electricity networks are not overloaded.

Introduction

Life expectancy (1) and economic growth (2) in hot/humid climates have improved with the mass deployment of air-conditioning (3). But neither traditional vernacular designs (4, 5), nor contemporary "bioclimatic" solutions (6) should be disregarded without reason. Depending on local circumstances some refrigerative air-conditioning may be necessary to complement more efficient modes of providing cool relief (7, 8). Yet the growing demand for air-conditioning can contribute to deadly power blackouts (9), such that air-conditioning becomes inoperable.

Wicked problems can be circumvented by "thinking outside the box". The present work is framed in response to the modern paradigm shift to insulate buildings with the ambition of improving winter comfort without increasing demand for heating that could be provided by boilers or furnaces. Unintended problems can arise in summer as insulation traps heat and humidity from cooking and occupants' respiration. So, the sub-tropical Australian State of Queensland's sustainable development code (10) awards energy efficiency rating credits when a dwelling includes an outdoor living area covered from sun and rain, yet openly alfresco – such as a veranda. QDC only credits outdoor living areas if they are directly accessible from indoor spaces (lounge, kitchen, or dining room) and fully covered by an impervious roof. Additional credits are awarded if the outdoor living area is covered by a ceiling fan suspended below an insulated roof.

Australian governments (including the state of Queensland) require dynamic simulations of new building designs that assess both the heating and cooling loads within the building envelope (11), and such software has the potential to assess overheating risk indoors (12). Subsequently the UK Government has introduced building regulations to encourage external shading of windows and cross flow ventilation in preference to air-conditioning – complicated by demands to improve standards of insulation in order to minimize demand for heating in winter (13).

Naturally ventilated buildings and sheltered outdoor living areas such as balconies and verandas (14, 15) may provide some relief when air-conditioned buildings fail to provide resilient cooling during extreme heatwave events or power grids failures (16). So the present work aims to map the global bioclimatic limits of passive and low energy alternatives to air-conditioning, based on ground-truth observations, and to consider local trends. Accepting that there may be poorly designed dwellings prone to dangerous overheating that demands air-conditioning while neighbouring parks and gardens may provide passively cool relief – the current work uses a readily computed measure of heat stress to identify the practical limit of shaded outdoor living areas as an alternative to air-conditioning. Basically to think outside the building envelope, yet under shade.

Wet bulb globe temperature (WBGT) and heat stress flag categories

Consider a counterfactual approach to design of air-conditioning by considering passive and low energy alternatives (17). That research commenced by assuming air-conditioning is desirable (18) when mean daily outdoor air conditions (typically circa 9 AM) rise above 24°C dry bulb temperature or 9.4 °C wet bulb temperature -except for conditions when lower energy cooling may suffice (not exceeding 27°C dry bulb or 24 °C wet bulb). That complex threshold was found to not exceed 25.6°C wet bulb globe temperature in shade at the time of daily maximum ($WBGTs_{max}$).

25.6°C (78°F) WBGT is the lowest threshold (Table 1) used in military and athletic settings to assess environmental heat stress and determine safe activity levels, which triggers a "White-flag" warning – when healthy individuals can safely exert themselves as long as they can rest in shade and remain hydrated, while elders and unhealthy people should still be more concerned. A "Yellow-flag" heat stress warning is declarable if wet bulb globe temperature rises above 29.4°C (19), which is when "moderate risk" precautions (such as rest breaks and rehydration) become more important in the management of risk of heat-related illnesses (20). Military guidelines exclude "white-flag" from heat stress catagories and rather lower their threshold for "green-flag" conditions to 26.7°C (80°F).

Table 1: Thresholds of White-, Green-, Yellow-, Red-, and Black-Flag WBGT

White ≥ 78°F	Green ≥ 82°F	Yellow ≥ 85°F	Red ≥ 88°F	Black ≥ 90°F
25.6 - 27.7°C	27.8 - 29.4°C	29.5 - 31.1°C	31.2 - 32.1°C	32.2°C -
very low risk	low risk	moderate risk	high risk	extreme risk

US military training guidance based on wet bulb globe temperature (20).

WBGT is defined by equation 1.

$$\text{WBGT} = 0.7 \times \text{natural wet bulb} + 0.2 \times \text{globe temperature} + 0.1 \times \text{dry bulb} \quad \text{(equation 1)}$$

Where natural wet bulb is the temperature that a thermometer reads when the bulb is wrapped in a wet wick exposed to the micro-climate's air flow (or stagnation as the case may be).

Ambient air temperature is also known as the dry-bulb temperature and must be measured within a well-ventilated radiation screen, surrounded by louvres coloured white to reflect solar radiation while rejecting thermal radiation (21).

Globe temperature is the temperature that a thermometer encased in a lamp-black sphere would read when exposed to the direct solar and thermal radiation environment of

representative exposure of people in any particular microclimate (19). Globe temperature will closely approach the dry bulb temperature in situations where people are shielded from both thermal and solar radiation.

Equation 1 weights WBGT 70% with respect to the naturally aspirated wet bulb temperature observed in any microclimate of concern, while only 30% is weighted with respect to the combined impact of the radiant (black globe) and ambient dry bulb temperatures in the microclimate of the occupants. It should be noted that natural wet bulb temperature vary a few degrees above the fully aspirated psychrometric wet-bulb temperature which is readily calculated from pressure, relative humidity and dry-bulb ambient temperature using thermodynamic equations of state of moist air (22, 23).

Well-designed shelters and shade trees can provide micro-climates where in the WBGT improves by eliminating both solar and thermal radiation while natural wet bulb temperature drops to approach aspirated psychrometric wet bulb temperature. Therein results the shaded wet bulb globe temperature (WBGTs) given by equation 2.

$$\text{WBGTs} = 0.7 \times \text{psychrometric wet bulb} + 0.3 \times \text{dry bulb air temperature} \quad \text{(equation 2)}$$

WBGTs is readily computed from the annuals of meteorological observations, so we can determine where extreme heat and humidity have exceeded assumed safe threshold values (17). The policy of raising a yellow flag whenever WBGT breaches 29.4°C (85°F) has for half a century required officers to dismiss unacclimated recruits from training in dangerous heat (24). Meanwhile acclimated healthy soldiers could continue with a cycle of hydration and rest breaks, while activities were further limited when a red-flag heat stress warning was raised if WBGT breached 31.1°C (88°F).

A high-humidity example of red-flag conditions is 34°C shaded dry bulb (operative temperature) while wet bulb temperature is 30°C. Berkley Comfort Tool https://comfort.cbe.berkeley.edu/ (25)

suggests this particular breach of what we are considering "red flag" conditions corresponds to 75% relative humidity, and that ISO 7730 (26) predicted mean vote (PMV) would be 1.47 with 49% percent of population dissatisfied (PPD) – subject to 4 m/s air speed with local control for persons lightly dressed (0.36 clo) and resting (1 met). According to the same website (25) entering a 33% relative humidity breach of red-flag conditions (41°C dry bulb / 27°C wet bulb) with the same air-flow and lightly dressed resting scenario results in 3.52 PMV with 100% PPD – uncomfortably hot, but such hot-dry conditions are readily mitigated by spray misting (27) if fresh water is available.

International Standard ISO 7243:2017 (28) assesses thermal stress of indoor and outdoor environments, depending on metabolic rate of activities and acclimation of workers on the basis of Wet Bulb Globe Temperature (WBGT). Protective clothing can trap heat and humidity, elevating risk (Annex F of ISO 7243:2017) several degrees below what a safe WBGT would otherwise be. Rehydration being necessary for healthy evaporative cooling via sweat glands, individuals suffering from anhidrosis (either genetic or a side effect of certain drugs/medications) are unable to sweat, and thus limiting thermoregulatory ability. Without reference to flags or colour codes, Annex A of ISO 7243:2017 lowered thresholds for unacclimated people exercising at "low metabolic rate" (150 Watts) slightly to 29 °C WBGT, while acclimated persons are limited to 30 °C WBGT. But ISO 7243 "does not take account of any effect related to body size or similar characteristic, e.g. obesity, height, weight". Table 2 summarises effective $WBGT_{eff}$ as informative guide for local policy makers, where they state that "values will generally differ by ± 1 °C".

Table 2: $WBGT_{eff}$ thresholds for work at five metabolic rates

Descriptive Class	Metabolic Watts	acclimated $WBGT_{eff}$	unacclimated $WBGT_{eff}$
0 Resting	115	33 °C	32 °C

1	1 Low	180	30 °C	29 °C
2	2 Moderate	300	28 °C	26 °C
3	3 High	415	26 °C	23 °C
4	4 Very high	520	25 °C	20 °C

5 Adapted from informative Annex A, ISO 7243:2017 (28) Table A.1

6 Passive survivability during heat wave power blackouts can be certified (29) by psychrometric
7 analysis of temperature, humidity and thermal radiation if dwellings' WBGT doesn't exceed
8 28°C. Such conditions mostly coincide with white-flag heat stress conditions and only
9 fractionally overlap green-flag conditions (20). Meanwhile, passive survivability of non-
10 residential buildings is recognized for yellow-flag conditions up to 31°C WBGTs (29). A tenth of
11 degree above is the threshold of outdoor conditions announced by raising a red-flag at athletic
12 and military training facilities (30), in which case occupants would be advised to cease activities
13 and seek cooler relief.

14 Intermediate preventive measures (breaks with refreshments) are recommended for lightly
15 dressed activities during green-flag conditions when WBGTs breach 27.8°C (82°F), but un-fit
16 and non-acclimated individuals should (31) spend at least 50% of their shift repeatedly resting
17 and rehydrating. The threshold of extreme risk for adapted healthy individuals ("black-flag"
18 conditions) is 32.2°C (90°F) WBGT, which can result in uncompensable heat stress even while
19 resting and rehydrating continuously in shade (32).

20 During the second decade of this century a consortium of physiologists (33) developed a
21 complex human comfort model – Universal Thermal Climate Index (UTCI) to consider risk of
22 heat as well as cold (34). UTCI is based on a heat balance model of the human body does not
23 take account of individuals' adaptability in terms of metabolic rates and clothing (35), but
24 recently has been considered, together with WBGT in many applications (36). Meanwhile
25 WBGT has decades of institutional inertia in regulation of workplace health and safety – as

WBGT can be verified the field, while UTCI requires data that are often unavailable in meteorological data sets.

Drawing in gridded model output and weather station observations the charity Climate Change Heat Impact & Prevention (Climate CHIP) Hothaps software (37, 38) calculates trending of annual maxima of both WBGT and UTCI in shade, while UC Berkley Center for the Built Environment (CBE) Clima Tool synthesizes typical 8760 hour summaries of UTCI together with other parameters, but neglects WBGT (39). CBE Clima Tool requires user input of a weather file of the EnergyPlus format (40) that have been assembled from of historic weather ground truth and grided products to provide UTCI hourly comparisons, either in sun or shade, and either in either in or out of wind. Unlike UCLA Climate Consultant (41) – another tool that uses EnergyPlus weather files – CBE Clima does not suggest design strategies such as evaporative cooling or air-conditioning.

Climate CHIP reports WGBT in sun or shade, based on daily maximum conditions. Furthermore, the Climate CHIP website provides trends and standard estimate of error of linear regressions with respect to the timeseries of observations (42), which is similar to the current study – following from previous studies of bioclimatic screening alternative options for heating and cooling (17, 43).

Previous work of the present author (17, 44), as well as Climate CHIP use Global Summary of the Day (GSOD), which is a global database that consists of surface observations archived at the NOAA's National Centers for Environmental Information (NCEI) (45, 46). GSOD (47) is a data repository which summarizes daily weather elements computed from members of the World Meteorological Organization (WMO). GSOD serves mean values of temperature, dew point temperature, and station pressure, as well as maximum and minimum dry-bulb temperature. GSOD undergoes quality controls to remove errors that might be present among original observation data from thousands of meteorological stations around the world since

1973. There were 12,159 station summaries during year 2024, having increased from 8,418 during year 1975 with a peak of 12,262 during year 2020. Some stations commenced observations later, while others closed during the half century 1975-2024, which intersected over 21,000 locations.

Objectives of the current study

The current study aims to provide a global reanalysis of the years 1974-2024 accessible from GSOD of all locations that were determined to be places where air-conditioning was deemed to be desirable, but not essential for adapted healthy individuals who are able to rest and rehydrate in shade during years 1987-2020 (17, 44, 48). As in those studies, the current research assumes yellow-flag heat stress conditions (29.5 to 31.1°C WBGT) are undesirable but occasionally tolerable up to 10 days per year if precautions are implemented. Where ten or more shaded yellow-flag days ($WBGTs_{max} \geq 29.5$°C) were experienced in years that are hotter than normal, then such places are deemed to be localities where planning access to air-conditioning or other means of cool relief is a matter of public health. In stationary climates, hotter-than-normal is deemed to be inclusive of one standard deviation of the inter-annual variability of the number of days that maximum daily WBGTs equals or exceeds 29.5°C (78°F). In cases where there is a statistically significant trend, then hotter-than-normal is assumed by adding the latest linear estimate plus the standard estimate of error of the inter-annual variability of the number of days that maximum daily WBGTs equals or exceeds 29.5°C (78°F) – the yellow-flag threshold.

The current study does not dispute that vulnerable individuals may have a legitimate need for relief from white-flag conditions – at a threshold of 25.6°C WBGTs (20). So, the current research focuses on reanalysis of locations that were found in a previous study (44) to have experienced more than 10 white-flag days in a hotter-than-normal year, but not more than 10 yellow-flag days in an average year. Thus, the present research is working with a cohort of the

GSOD network as analysed during the years 1987-2020 that is hereby referred to as the "green-yellow" cohort, where there were numerous green-flag and yellow-flag days during hotter-than-normal years. This cohort includes some locations that experienced more than 10 yellow-flag days in a hotter-than-normal year - recording some extreme summers by year 2020. Because year-on-year averages did not reveal such cases, we need to consider extremes that emerge from the noise of interannual variability. For example, the El Niño Southern Oscillation was a known cause in Australia (49), so 20th century air-conditioning design methods have added one standard deviation of the inter-annual variability to the year-on-year average of the 10th hottest daily maximum each year of observations (50).

White-flag exposure up to nine days per annum only occasionally breached into green-flag conditions (27.8 to 29.4°C WBGT) - coinciding with Table 2 which outlines recommendations for unacclimated healthy individuals to rest while acclimated individuals should moderate their exertion. Yellow-flag exposure inherently includes breaches of green-flag exposure, so the two have been lumped together for reanalysis of the latest observations and trending forecasts to assess where access to air-conditioning might become essential for all individuals circa the year 2050.

Recent re-evaluation of published results of global analysis of 34 years through 2020

Recently accepted paper for CIBSE Technical Symposium 2026 (44) documents how GSOD (47) analysis of the 34 years 1987-2020 (17) resulted in openly available tabulations (48) and graphics (51). The result delineates the "green-yellow" cohort sample of the global population that is considered in the current study, expanding the analysis to consider all accessible observations during the 50 years 1975-2024. The cohort included those (n†=4,661) weather stations with identified geographical coordinates for which the 34-year analysis (1987-2020) had Wsd†≥10 but YsD<10, using the MATLAB m-file "green_yellow.m" (supporting on-line materials).

The green-yellow cohort generated via the script green_yellow.m included a few stations from the hotter margin of the blue-symbolled regions that were assessed to experience ten or more "white-flag" WBGTs-days in hotter than normal year (WsD†), even if some of these stations averaged less than ten "average" white-flag WBGTs-days (Wsd<10) averaged through the annals ending 2020. On the other extreme, stations with potentially more than 10 yellow-flag-days in a hot year (YsD†>10) could be included in the green-yellow cohort as long as they averaged less than 10 yellow-flag WBGTs-days (Ysd<10) through the annals ending 2024. The cohort criteria are given in equation 3.

$$(WsD\dagger \geq 10 \quad \text{and} \quad Ysd<10) \quad \text{or} \quad (0<Ysd<10) \qquad \text{(equation 3)}$$

The value of white-flag-days in a hotter than normal year, WsD†, was calculated differently if there was a "NaN" (not-a-value) entered in a particular station's report in the "WsD" column of the previously published supporting on-line material (48) – in which case the value from the column "std_W" (standard deviation of the interannual variability) was added to the value from the column "Wsd" (assumed stationary mean) to estimate a nominal upper bound (WsD†). But if a numerical value was found in the "WsD" column, then there was statistically significant trend (17) and so the value in the column "SEE_W" (standard estimate of error) was added to the trended estimate of the mean at the year denoted in the "stop" column (the last year of observations) to estimate a nominal upper bound (WsD†) at the latest year of the annals.

Additionally there are a couple of locations (Hervey Bay, Australia and Toledo, Spain) with negative trends that just dipped their estimated WsD† below the 10 day per annum threshold at the last year (2020) after their earlier scatters peaked above – so these two were manually added to the green-yellow cohort for consideration of the more extensive period of annuals (methods part 2).

The nominal upper bound of yellow-flag-days (YsD†) at the latest year of the annals was taken from the sum of the values from the "SEE_Y" and "YsD" (unless YsD was NaN, in which case the values from "std_Y" and "Ysd" were summed). So, a couple of manual inclusions were drawn from the high side – these being Beauregard Airport, Louisiana and Los Mochis Airport, Mexico. The former averaged just 10 Ysd that was trending down to 5 YsD† at year 2020, while the latter's Ysd average of 14 was trending down to 5 YsD† by 2020.

Methods part 1: Reanalysis of sites previously classified "green-yellow" medium-high risk

GSOD meteorological observations were downloaded from the NCEI website, but some stations' data were of insufficient quality and/or resolution to evaluate annual count of days of WBGTs exposure. For example, it is impossible to determine wet-bulb (nor WBGT) without records of relative humidity or dew point, and an annual rate was not considered without at least 300 days of both dry- and wet-bulb observations.

The green-yellow cohort list of observation stations has now been re-processed with reference to GSOD (47) throughout the half-century 1975-2024 by the same published methods (17) as used to generate the previously published results (48), but with some additional algorithms detailed here and further below in methods part 2. The modified MATLAB script WB_5Nov2025.m now calls a modified WBloop_5Nov2025.m which in turn calls script WBGT_Fs_try2.m, which subsequently calls the MATLAB File Exchange's Mann-Kendall Tau-b with Sen's Method "ktaub.m" (52) .

This produces five files that log the white-, green-, yellow-, red-, and black-flag WBGTs days (RESULTSflagW, RESULTSflagG, RESULTSflagY, RESULTSflagR, RESULTSflagB).

Each line of these files registers the Placename, WMO and Weather Bureau Army Navy (WBAN) identifier numbers, as well as the first of the WBGT flag (W,G,Y,R, or B) and that flag's

lower threshold WBGTs in both °F and °C). Each line also tabulates trend analysis [trend_direction, sig, Z, tau, taub], where "trend_direction" is either increasing or decreasing based on "sig" the two-tailed p value, "Z" score, "tau" the Mann-Kendall coefficient not adjusted for ties, and "taub" the Mann-Kendall coefficient adjusted for ties.

Curve fitting analysis results are included to the right of Mann-Kendall trend results: [slope, intercept, sse, R2, dfe, adjR2, rmse, SEE, latest]. Where the linear regression slope, intercept, error sum of squares, R^2, degrees of freedom, adjusted R^2, root mean square error, standard estimate of error, and latest year of assessment are also tabulated.

Methods part 2: Trended projection of "green-yellow" cohort to question risk circa year 2050

Where methods part 1 found stations to have a statistically significant trend, then projections of risk were estimated at these locations circa year 2050. This method was attempted with each call of a script 'WBGT_Fs_try2.m' that invokes MATLAB's 'predint' after prerequisite linear regression models of the annual white-, green-, yellow-, red-, and black-flag-days (Wsd, Gsd, Ysd, Rsd, and Bsd) observed each year of the annals versus the year as the independent variable.

The upper bound of 95% confidence interval projection to year 2050 (WsD‡,GsD‡,YsD‡,RsD‡,BsD‡) would not "normally" be exceeded – assuming a perpetuation of the historic trend of the annual count of peaks-over-threshold. But this also depends on assuming a Gaussian distribution of interannual variations around the non-stationary predicted forecast at year 2050, if it were by-chance "averages" (Wsd, Gsd, Ysd, Rsd, Bsd) rather than the usual scatter hotter or cooler.

Give these idealistic assumptions, these projections to question risk circa year 2050 cannot be considered conclusive forecasts. They should rather be offered as a guide for on-going

monitoring and more advanced application of extreme value statistics in cases trending toward the hot side.

MATLAB script "WBGT_Fs_try2.m" stacks the annals of WBGTs-flag-days. For example , the "Red" annals of red-flag days per annum include concurrent daily flagging of black-flag WBGTs. The vector of each WBGTs flag ("Black", "Red", "Yellow", "Green", "White", "Blue", "Cyan", and "Cooler") as well as the vector of the timestamps "Year" are abbreviated by removing any rows of without any observations – so that the sequence of "Year" may have gaps in order to avoid ingesting zeros into the analysis unless that is some real number of WBGTs observations (rather than NaN). Note that WBGT cannot be determined without humidity observations. Subject to the forgoing, the "WBGT_Fs_try2.m" script applies the following command lines to prepare for curve fitting the annals of red-flag WGBTs where Year and Red are independent and dependent data vectors.

```
[RtData, RyData] = prepareCurveData(Year, Red );          (command line 1)
[Rfitresult, Rgof] = fit( RtData, RyData, ft );           (command line 2)
RciE = predint(Rfitresult,enddate);                       (command line 3)
```

Command line 1 reshapes both into column vectors, removing NaN or Inf values, to ensures they're suitable for fitting. The output "RtData" and "RyData" are cleaned and formatted versions of "Year" and "Red". So that the script can then apply the second command line to fit red-flag WBGT trend. Command line 2 "fit" performs curve fitting using the cleaned data, while "ft" is the fit type ('linear') that was pre-defined to ensure a linear trending model is used. Output "Rfitresult" is the fitted MATLAB model object, while "Rgof" are goodness-of-fit metrics (SSE, R-square, RMSE, etc.). And finally, use the third command line to predict the 95% confidence interval at the enddate 2050:. Thus MATLAB "predint" calculates 95% "confidence" bounds for projections from the fitted model, where "Rfitresult" identifies the fitted model

generated in the MATLAB workspace, while ‘‘enddate’’ is the future year for forcasting (which has been preset as year 2050). Thus ‘‘RciE’’ returns a two-element vector: the lower and upper bounds of projection to ‘‘enddate’’, with 95% expectation.

Forecast analysis is logged with respect to white-, green-, yellow-, red-, and black-flag WBGTs in results files (RESULTSflagW, RESULTSflagG, RESULTSflagY, RESULTSflagR, RESULTSflagB). Wherein 95% expectation interval ‘‘95L_fwd’’ ‘‘95U_fwd’’ of year 2050 projections are tabulated to the right of the last year of observation and the future year (2050). A spreadsheet is then to consider significant trend results founded by at least as many years of observations as projection forward from the latest observation to 2050. Such projected reclassification of exposure categories is marked within Figures 6, 7, or 8 by circumscribing a triangle around smaller coloured markers that denote their previously risk classifications.

Methodological framework (revision of 2021 version of MATLAB script and functions)

WB_5Nov2025.m calls function WBloop_5Nov2025.m to process historical meteorological data from NOAA’s GSOD dataset to evaluate climate-driven HVAC needs and human heat stress risks. These are revisions of the script WB_2021_u_.m that called the function WBloop_2021_u_.m (48) as compared in Table 3.

Sequentially working through their assigned station list, these scripts download and processes daily weather data (temperature, dew point, pressure) for given WMO/WBAN station identifiers. Both versions calculate heating and cooling degree days, psychrometric conditions, Wet Bulb Globe Temperature (WBGT) classifications, and assess the potential for energy savings through alternative cooling strategies. Both versions analyse historical meteorological data, including:

- Filling short missing data gaps using interpolation techniques.
- Convert temperatures to Celsius and calculate wet bulb from dewpoint and pressure.
- Compute WBGTs using a weighted average of dry bulb and wet bulb temperatures.

- Classify days into WBGTs flag threshold categories (white, green, yellow, red, black).
- Uses Durbin-Watson tests to assess autocorrelation in residuals.

However, the 2021 version (30) focused on batch processing every available station during 34 years (1987-2020), summarizing results into three text files (RESULTSout, RESULTSrates, RESULTSstats). While the 2025 version deepens the analysis for a specified cohort of selected stations, extending the period of assessment to cover years 1975-2024 with deeper analytic assessment, including:

- Adapts Kjellstrom 4+4+4 method (53) for estimating WBGTs flag exposure hours.
- Assesses mean daily conditions to classify days as "Safe", "Risky", and "Deadly" (48, 54).
- Mann-Kendall trend analysis (52) of WBGTs flag exposure days per annum.
- Matlab curve fitting WBGTs flags' confidence interval of projections out to year 2050.

WBGT_Fs_try2.m analyzes annual WBGT flag days (White, Green, Yellow, Red, Black) for a given weather station to detect trends using both linear regression and Mann-Kendall non-parametric tests, forecast future values (to 2050), and generate summary statistics and visual plots. It reads from each station's subfolder *_WBGT.txt files containing annual counts of days in each WBGT flag category, and removes rows with all zeros (no data). Then it computes cumulative counts (such as White = white + green + yellow + red + black, and Yellow = yellow + red + black). Then it applies a linear model (fitlm) to each flag category vs. year, extracting slope, intercept, R^2, adjusted R^2, RMSE, SEE, and 95% confidence intervals at the forecast year (2050). It also applies a Mann-Kendall Trend Test by calling ktaub.m for each flag category to compute Tau, Tau-b, Z-score, p-value, and determines if the trend is increasing, decreasing, or insignificant. Finally, it projects trends to the specified forecast year (2050), reporting the upper and lower 95% confidence bounds from MATLAB's Curve Fitting Toolbox

predint function. Visualization is achieved by creation of graphics in each station's output folder which includes scatter plots of annual flag days, fitted trend lines with confidence bands, and annotated with trend direction and forecast ranges.

Table 3: Comparison of original 2021 version and 2025 revised MATLAB scripts and functions

	2021 original	2025 revision
Control script	`WB_2021_u_.m`	`WB_5Nov2025.m`
Function	`WBloop_2021_u_.m`	`WBloop_5Nov2025.m`
Additional functions		`WBGT_Fs_try2.m & ktaub.m`
Common functions	`psych.m & H2O_psych.m`	
Station Selection	`isd-history_2021.csv`	`isd-selection.csv`
Common references	`stations.txt & placenames.txt`	
Start-Stop	1987-2020	1975-2024
Output Files	`RESULTSout`, `RESULTSrates`, `RESULTSstats`	Adds `RESULTSmore`, `RESULTSflagW/G/Y/R/B`
WBGTs Flags	Only White and Yellow	Full 5-color WBGTs flag classification (White, Green, Yellow, Red, Black)
Trend Analysis	Linear regression with Durbin-Watson test (RESULTSstats)	Adds Mann-Kendall flag trends, forecast to 2050, so called "confidence intervals", and significance flags (`RESULTSflagW/G/Y/R/B`)

	2021 original	2025 revision
Control script	`WB_2021_u_.m`	`WB_5Nov2025.m`
Function	`WBloop_2021_u_.m`	`WBloop_5Nov2025.m`
Additional functions		`WBGT_Fs_try2.m & ktaub.m`
Common functions	`psych.m & H2O_psych.m`	
Station Selection	`isd-history_2021.csv`	`isd-selection.csv`
Common references	`stations.txt & placenames.txt`	
Forecasting	Not included	Adds slope-based future projection with 95% "confidence" intervals

Results

The n=3661 land locations identified as "green-yellow" cohort of the 15,542 land-based station analysis of the 34 years 1987 through 2020 included a coincident gpw_v4 population of 3,404,731 out of the 9,124,984 coincident population representing a global sample. Hence the "green-yellow" cohort was a 22.3% subset of all land-based stations, with 28.2% of the population.

Results are summarized in Figures 1-8 as maps with scatter-plot symbols which are shaped and coloured according to Table 4. Meteorological stations that did not breach any of these criteria or where annals were of insufficient quality to interpret are not plotted. Note that urban heat islands are rarely monitored by long term meteorological observations, and so heat stress is likely to be worse in urban centres than the surrounding datapoints indicate. WsD† represents the number of days in a hotter-than-normal year that "white flag" conditions were breached, while Wsd represents the number of days breached in an average year. Likewise, YsD†

represents the number of days in a hotter-than-normal year that "yellow flag" conditions were breached, while Ysd represents the number of days breached in an average year. Per annum ("pa") classifications account for exposure in hotter-than-normal years. Herein star shaped symbols (WsD† and YsD†) denote where the addition of one standard deviation above interannual average (Wsd and Ysd) or standard estimate of error added to linear regression trend to the last year increased map colour classification thresholds in hotter-than-normal years. Otherwise, circle symbols denote where interannual average (Wsd and Ysd) share the same map colour classification as hotter-than-normal years (WsD† and YsD†). There are five map colour classifications as set out in Table 4, with further elaboration below.

Table 4: Map symbol shape and colour classifications according to WBGTs exposure in shade

Colour	stars	circles	Map colour category (exposure / hotter-than-normal year)	Seasonal Exposure
Cyan	1≤WsD†<3	1≤Wsd<3	"white flag" WBGTs 25.6 to 27.7°C possible 1 or 2 days	1. Lowest
Blue	3≤WsD†<10	3≤Wsd<10	"white flag" WBGTs 25.6 to 27.7°C possible 3 to 9 days. May include green-flag days.	2. Lower
Green	10≤WsD†	10≤Wsd	"white flag" WBGTs 25.6 to 27.7°C possible 10 or more days, but less than 3 yellow-flag days. May include green-flag days.	3. Medium
Yellow	3 ≤YsD†<10	3 ≤Ysd<10	"yellow flag" WBGTs 29.5 to 31.1°C possible 3 to 9 days	4. Higher

Red	10≤ YsD†	10≤ Ysd	"yellow flag" WBGTs 29.5 to 31.1°C on 10 or more days. May include red-flag days.	5. Highest

Cyan stars and circles indicate where WBGTs in shade were expected to have reached "white-flag" conditions one to four days pa. Cyan might represent where only the most vulnerable individuals require active cooling relief, while most others would cope by resting in well-ventilated shade.

Blue stars and circles indicate where WBGTs in shade were expected to have reached "white-flag" conditions five to nine days pa. Blue might represent where a larger proportion of elderly or unhealthy individuals could benefit from active cooling relief during extreme heat events.

Green stars and circles indicate where WBGTs in shade were expected to have reached "white-flag" conditions ten or more days pa among which one to four reached into "yellow-flag" conditions. These locations experience a number for days including "green-flag" conditions. Green suggests where most healthy individuals could cope with heat by staying in shade and regularly rehydrating.

Yellow stars and circles map markers indicate where WBGTs in shade were expected to have reached "yellow-flag" conditions five to nine days in a hotter than normal year. Yellow map markers suggest where a smaller proportion of healthy adapted individuals might be able to cope without air-conditioning if they can regularly rest and rehydrate under breezy shade, while green map markers indicate where there were fewer "yellow-flag" days – yet numerous "green-flag" days.

Red stars and circles indicate where WBGTs in shade were expected to have reached "yellow flag" conditions ten or more days pa, without specifying if "red flag" conditions were reached.

Many locations indicated by red symbols suffered many days of "red-flag" conditions, and not excluding the possibility of instances of "black-flag" WBGTs conditions.

Results of classifications based on 1987-2020 annals

Geographic coordinates were available for 16,532 of the 16,582 weather stations previously analysed https://doi.org/10.5518/967 (48) from the annals of 1987-2020. Of these, the total coincident population (gpw_v4) (55) was 9,124,984 inhabitants, representing a sample of global population biased by proximity within approximately one km grid cells of meteorological stations.

There was no overheating risk (WsD†<1) at 7,050 stations coincident with 24% of the population , to be mapped with the colour magenta. Generally mapped in the colours cyan and blue, moderate white-flag WBGTs days (1≤WsD†<10) were observed at 2,943 stations coincident with 17% of the global population sample. Increased overheating risk is generally plotted with green and yellow symbols where (10≤WsD† while Ysd<10) at 4,696 stations coincident with 38% of the sampled global population. Red symbols generally denote where exposure to humid overheating was highest (10≤Ysd), at 1,323 stations coincident with 20% of the global population sample. But if the threshold for the highest risk is lowered to include hotter than average years (10≤YsD†) then the higher risk stations totalled 2,078 coincident with 27% of the global population sample.

Partially answering the question implied by the title of this paper, accessibility to air-conditioning during heat events was essentially a necessity for all members of the population inhabiting the higher risk area (mapped by red symbols). Meanwhile increasing proportions of population could have tolerated heat where risk was lower (decreasing risk from yellow, green, and blue, to cyan).

Reanalysis of the most recent half century of annals (1975-2024)

The 3,661 "green-yellow" cohort of meteorological stations that have now been reanalysed had a total population coincident with one km cells of GPWv4 (56) of 3,404,731 persons. Geolocation was available for 15,542 stations of the previous global analysis (17), with a coincident population sample of 9,124,984 within the GPWv4 one km grid. Consequently, the "green-yellow" GSOD stations represents 37% of the global network of meteorological ground truth during 1987-2020.

Tables 5 and 6, and Figures 1-8 present results of reanalysis of stations coincident with the global population "green-yellow" cohort (10≤Wsd while YsD†<10) based on years 1987-2020 as queried from GSOD. This year's access of the GOD website was successful to download sufficient data for 4,657 of the "green-yellow" stations for reanalysis of whatever was available during most recent half century of annals (1975-2024). As the previous research coincident GPWv4 population of the 4,696 stations (17) was 3,427,575 persons, and 3,404,248 is the coincident population of the 4,657 stations now available for consideration, there is now 99.3% coverage of a "green-yellow" cohort that represents 38% of the previous researched global population (17). Email conversations with GSOD staff were disrupted by this years' US Government shutdown, so it is expedient to proceed without the 39 recently inaccessible "green-yellow" weather stations' datasets. Instead, two stations just below the cooler threshold (10≤Wsd) and two more stations just above the warmer threshold (YsD†<10) where included in the current reanalysis, bring the total to 4,661 stations that are coincident with 3,404,731 population from GPWv4. These four borderline cases (Toledo Spain, Hervey Bay Australia, Beauregard Louisiana, Valle del Fuerte Mexico) had experienced many "green-yellow" years during 1987-2020, but were locally cooling. For example, Beauregard's long term average Ysd was just on 10, while YsD† was down to 7, while Valle del Fuerte's Ysd was 14, but YsD† was only 5. Thus, two barely "red" and two barely "blue" stations have joined the cohort.

The final "green-yellow" cohort (n=4,661) was prepared for reanalysis over the latest half-century including year 2024 to check if risk of overheating has changed, and to project forward to estimate risk circa year 2050. Comparison with alternative classification of these stations is presented in Table 5, where the period queried from GSOD was either the half century concluding 2024 (1975-2024), or the 34 years concluding 2020 (1987-2020). Refer to supporting on-line material for the detailed tabulations of which range of years each station was reported by GSOD. From each temporal sample, Table 5 breaks down risk classification by three schemes –average years, hot years (denoted by dagger †), and a hybrid. The hybrid classification counts are denoted with double dagger (‡) where risk categories below the "green-yellow" zone are based on average years while the higher risk category 5 is based on hot years – latest regression estimate plus SEE or, in the case of stations where there was no statistically significant trend, their average plus standard deviation.

Table 5: Alternative classifications of "green-yellow" cohort of 4,661 GSOD weather stations

magenta	cyan	blue	light green	deep green	yellow	red
risk 0	risk 1	risk 2	risk 3	risk 3½	risk 4	risk 5
1987-2020 n=4661 "green-yellow" hybrid‡ cohort (GPWv4 population 3,404,731)						
Ysd<1 & WsD†<1	**Ysd<1 & 1≤WsD†<3**	**Ysd<1 & 3≤WsD†<10**	**Ysd<1 & 10≤WsD†**	**1≤Ysd<3**	**3≤Ysd<10**	**10≤Ysd**
		n‡=2	n‡=2,018	n‡=1,483	n‡=1,156	n†=2
		474 p‡	1,378,727 p‡	1,080,376 p‡	945,145 p‡	9 p‡
		0.01%‡	40%‡	32%‡	28%‡	0.0003%‡
YsD†<1 & WsD†<1	**YsD†<1 & 1≤WsD†<3**	**YsD†<1 & 3≤WsD†<10**	**YsD†<1 & 10≤WsD†**	**1≤YsD†<3**	**3≤YsD†<10**	**10≤YsD†**

		n†=2	n†=1,329	n†=1,226	n†=1,358	n†=746
		474 p†	818,065 p†	828,162 p†	1,140,332 p†	617,699 p†
		0.01%†	24%†	24%†	33%†	18%†
Ysd<1 & Wsd<1	**Ysd<1 & 1≤Wsd<3**	**Ysd<1 & 3≤Wsd<10**	**Ysd<1 & 10≤Wsd**	**1≤Ysd<3**	**3≤Ysd<10**	**10≤Ysd**
n=2	n=41	n=727	n=1,250	n=1,483	n=1,156	n=2
36 p	25,501 p	458,651 p	895,014 p	1,080,376 p	945,145 p	9 p
0.001%	0.7%	13%	26%	32%	28%	0.0003%

1975-2024 reclassification of the n=4661 hybrid‡ "green-yellow" cohort (GPWv4 population 3,404,731)

Ysd<1 & WsD†<1	**Ysd<1 & 1≤WsD†<3**	**Ysd<1 & 3≤WsD†<10**	**Ysd<1 & 10≤WsD†**	**1≤Ysd<3**	**3≤Ysd<10**	**10≤Ysd**
	n‡=1	n‡=17	n‡=1,987	n‡=1,453	n‡=1,103	n†=100
	0 p‡	2,317 p‡	1,360,748 p‡	1,037,894 p‡	933,581 p‡	70,191 p‡
	0%‡	0%‡	40%‡	30%‡	27%‡	2%‡
	-0.00001%Δ‡	-0.05%Δ‡	0.5%Δ‡	1.2%Δ‡	0.3%Δ‡	-2.1%Δ‡

YsD†<1 & WsD†<1	**YsD†<1 & 1≤WsD†<3**	**YsD†<1 & 3≤WsD†<10**	**YsD†<1 & 10≤WsD†**	**1≤YsD†<3**	**3≤YsD†<10**	**10≤YsD†**
		n†=13	n†=1,246	n†=1,167	n†=1,406	n†=829
		2,022 p†	820,689 p†	787,803 p†	1,037,424 p†	756,794 p†
		0.06%†	24%†	23%†	30%†	22%†
		-0.05%Δ†	-0.1%Δ†	1.2%Δ†	3.0%Δ†	-4.1%Δ†

Ysd<1 & Wsd<1	**Ysd<1 & 1≤Wsd<3**	**Ysd<1 & 3≤Wsd<10**	**Ysd<1 & 10≤Wsd**	**1≤Ysd<3**	**3≤Ysd<10**	**10≤Ysd**
n=1	n=19	n=150	n=1,835	n=1,453	n=1,103	n=100

0 p	3,936 p	56,105 p	1,303,023 p	1,037,894 p	933,581 p	70,191 p
0%	0.12%	1.6%	38%	30%	27%	2.1%
0.001%Δ	0.6%Δ	11.8%Δ	-12.0%Δ	1.2%Δ	0.3%Δ	-2.1%Δ

Change of percentage population sample, delta figures (%Δ‡, %Δ†, %Δ) given in Table 6 summarize how the latest queried period (1975-2024) is characterised differently from the earlier queried period (1987-2020). All cases presented in Table 6 show how the 1987-2020 n=4661 hybrid‡ "green-yellow" sub-sample population can be reconsidered to dwell across each of the seven risk classifications: 0 (magenta), 1 (cyan), 2 (blue), 3 (light green), 3½ (deep green), 4 (yellow), 5 (red).

The two timeframes are nested, with the new timeframe starting 13 years earlier and concluding 4 years later than the previously analysed timeframe (1987-2020). So, potential impact of possible decadal climate change trends is somewhat offset. Yet, Table 5 results add up to show that the net change of the population representing risk categories 3-4 in the latest queried period (1975-2024) decreased 10.4%Δ based on average-year thresholds. 12.5%Δ of the represented population would be counted as dwelling in cooler risk classifications (risk 0-2 "magenta, cyan , blue" Wsd<10 and Ysd<1) while -2.1%Δ were subtracted from the hotter classification (risk 5 "red" Ysd≥10).

Table 5 results of both hot-year† and hybrid‡ classification schemes add up to show that the net change of the population representing risk categories 3-4 ("green-yellow") in the latest queried period (1975-2024) decreased 4.1%Δ† and 2.1%Δ‡, respectively. In both of those schemes, only 0.05% would be counted as dwelling in cooler risk classifications (WsD†<10 and YsD†<1), while the predominance of their risk categorisation shifted up (Ysd≥10 or YsD†≥10 according to the scheme).

Figure 1 presents a global map, plotting the hybrid‡ "green-yellow" subsample during years 1975-2024 with bolden symbols over the colour classification of risk categories 0-5 during years 1987-2020. Note that the legend tabulates the number of GSOD stations classified up from the lowest risk category (0 magenta) to the highest risk (5 red), counting hot-year† cases of each risk category with a star shaped symbol wherever they happen to override the average-year classification that are denoted by round shaped symbols. The current study is focused on the potential for change of previously moderate risk (3-4 green-yellow) locations. So, regions of the world that are not marked on Figure 1 by black outline bolden markers might be speculated (but are not confirmed) to remain as either the highest risk (5 red), or among lower risk categories (2 blue, 1 cyan, 0 magenta).

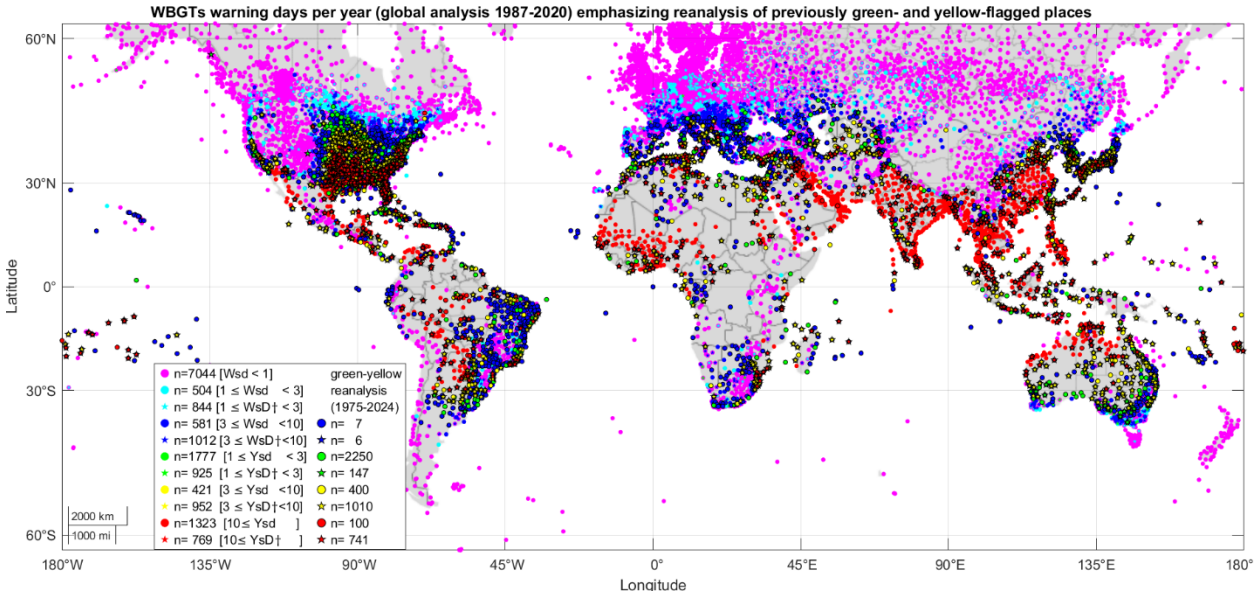

Figure 1: Embolden 1975-2024 reanalysis of previously green-yellow sites vs 1987-2020 results

Table 6 breaks down the sampled population percentage with respect to stations and their coincident 3,404,731 GPWv4 from the reanalysis of "green-yellow" locations. A further row indicates the share of global population by normalising with respect to the 9,124,984 GPWv4

population coincident with geolocated station list of the original analysis from which the hybrid "green-yellow" cohort was extracted based on years 1987-2020.

Table 6: White-, green-, yellow-, red-, black-flag day (Wsd, Gsd, Ysd, Rsd, and Bsd) trends

Trend	ΔWsd >0	ΔWsd <0	ΔGsd >0	ΔGsd <0	ΔYsd >0	ΔYsd <0	ΔRsd >0	ΔRsd <0	ΔBsd >0	ΔBsd <0
n=1526	n=772	n=142	n=1,237	n=75	n=385	n=22	n=82	n=11	n=18	n=4
Population (kp=1000p)	1,047 kp	1,417 p	1,220 kp	16 kp	523 kp	22 kp	195 kp	17 kp	38 kp	21 kp
share / 3.4047 Mp	31%	0.04%	36%	0.5%	15%	0.6 %	6%	0.5%	1%	0.6%
share / 9.1250 Mp	11%	0.02%	13%	0.2%	6%	0.2 %	2%	0.2%	0.4%	0.2%

Significant trends of WGBTs flag days found at n=1526 (1,492,154 GPWv4) of the n=4661 "green-yellow" (3,404,731 GPWv4) cohort of previous geolocated 15,542 stations (9,124,984 GPWv4).

Because of the inherent selection bias, global trends of change of per annum rates of WBGTs white-, red-, and black-flag days (ΔWsd, ΔRsd, and ΔBsd) could be under-represented here. So, the pertinent results to consider from Table 6 are regarding the trending of WBGTs green- and yellow-flag days per annum (ΔGsd and ΔYsd). Nearly 13% of the coincident geolocation sampled global population have been dwelling where ΔGsd > 0 (increasing), while almost half of that portion of the population (6%) are also experiencing statistically significant increasing

yellow-flag days per annum (ΔYsd > 0). Meanwhile about ½% of the representative global population is dwelling in "green-yellow" locations where there are green- and yellow-flag days were tending to be cooling.

An additional caveat to bear in mind is that only a portion of the population dwell where a meteorological station has served at least 25 years of observations, so projecting these trends forward to year 2050 could be considered far-fetched. And so, there is uncertainty of the proportion of global population experiencing significant changes in exposure to WBGTs flag warnings.

Higher resolution maps detail the reanalysis of the previous timeframe's hybrid‡ "green-yellow" during years 1975-2024 (Figures 2-8). These maps zoom into continental regions of USA, central South America, the Mediterranean, southern Africa, the Middle East, East Asia, and Australia. These maps mark hot-year† cases of each risk category with a star shaped symbol wherever they happen to override the average-year classification that are denoted by round shaped symbols. Meanwhile, in the limited number of cases where there is projection of plausible change of risk classification by year 2050, then a larger triangle of the appropriate perimeter colour circumscribes the current classification symbol. Results of forecast projections are only mapped where significant trending was determined by Mann-Kendall testing using Sen's method. Mention is made in the following text of those cases where a "green-yellow" station's historic annuals were at least as long as projecting forward from their latest full year observation forward to year 2050, and if trending to risk 10 yellow-flag days in a hot year (YsD†c2050≥10 marked by a red triangle).

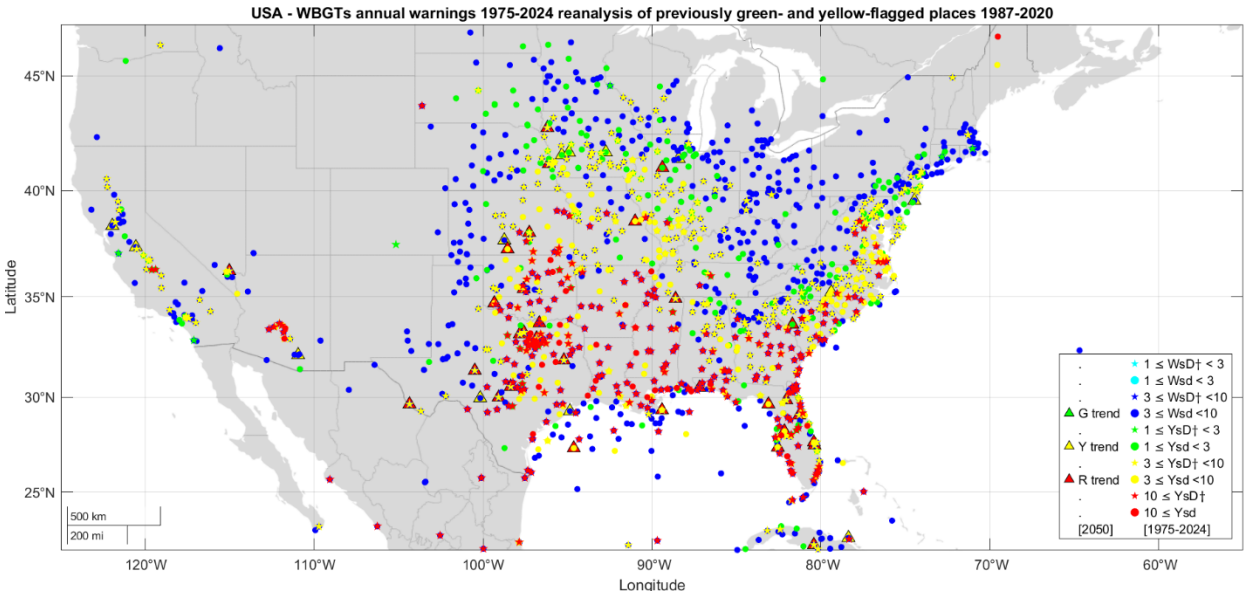

Figure 2: USA 1975-2024 reanalysis of previously green-yellow sites and 2050 projections

San Angelo Texas, Oklahoma City, Cross City Florida, and Medicine Lodge Kansas are the only green-yellow US locations trending with projections (54%, 54%, 64%, and 79%) less than their history with a red triangle (YsD†c2050≥10). Another such case is Cienfuegos Cuba (77% projection), while south beyond the frame of Figure 2 is Managua Nicaragua (73% projection).

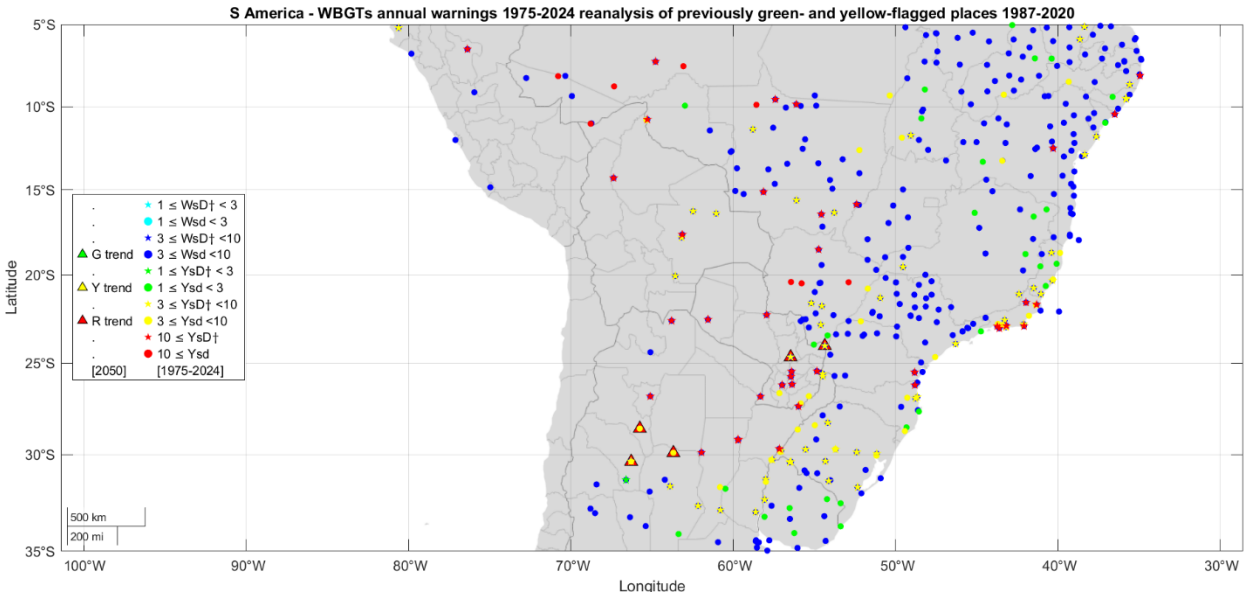

Figure 3: S America 1975-2024 reanalysis of previously green-yellow sites and 2050 projections

Catamarca, Chamical, and Villa de María del Río Seco (3 locations in Argentina) and San Estanislao (Paraguay), are locations marked with a red triangle in South America that are not projected more than their observational histories (54%, 94%, 100%, 97%- respective projections). Saltos del Guaira Paraguay is also marked with a red triangle, but that is based on 150% projection.

Meanwhile to the west of Figure 3 are Vele (Wallis & Futunaand) and also Faleolo (Samoa), which are trending (YsD†c2050≥10) with projections (82% and 100%) that are not more farfetched than the extent of their observational histories.

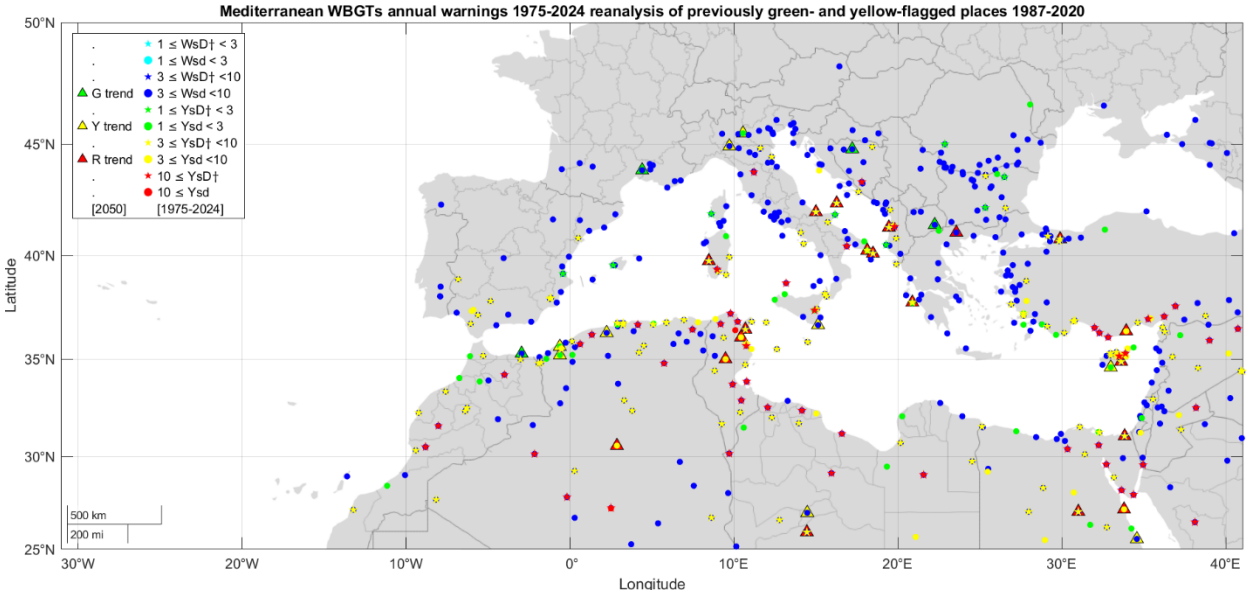

Figure 4: Mediterranean 1975-2024 reanalysis of previously green-yellow sites and projections

Four green-yellow Italian stations Lecce, Otranto, Termoli, and Cape Frasca Sardinia are marked with red (R trend YsD†c2050≥10) triangles based on projections 54%, 75%, 79% and 81%, respectively. Similarly, there are three Egyptian stations Asyut, Hurghada, and El Arish in the Sinai based on projections 71%, 79%, and 87%, respectively. Also, Sidi Bouzid Tunisia, Serres Greece, El Menia Algeria, Larnaca Cyprus, Silifke Türkiye, and Durrës Albania (61%,

56%, 57%, 57%, 57%, 68% projections). Meanwhile three Italian stations Izmit, Zakinthos, and Palagruza, Traghan Libya, and Tunisian stations Nabeul and Enfidha are also marked with red triangles, but it should be noted that their projections (300%, 193%, 108%, 225%, 127%, 180%) are relatively far-fetched.

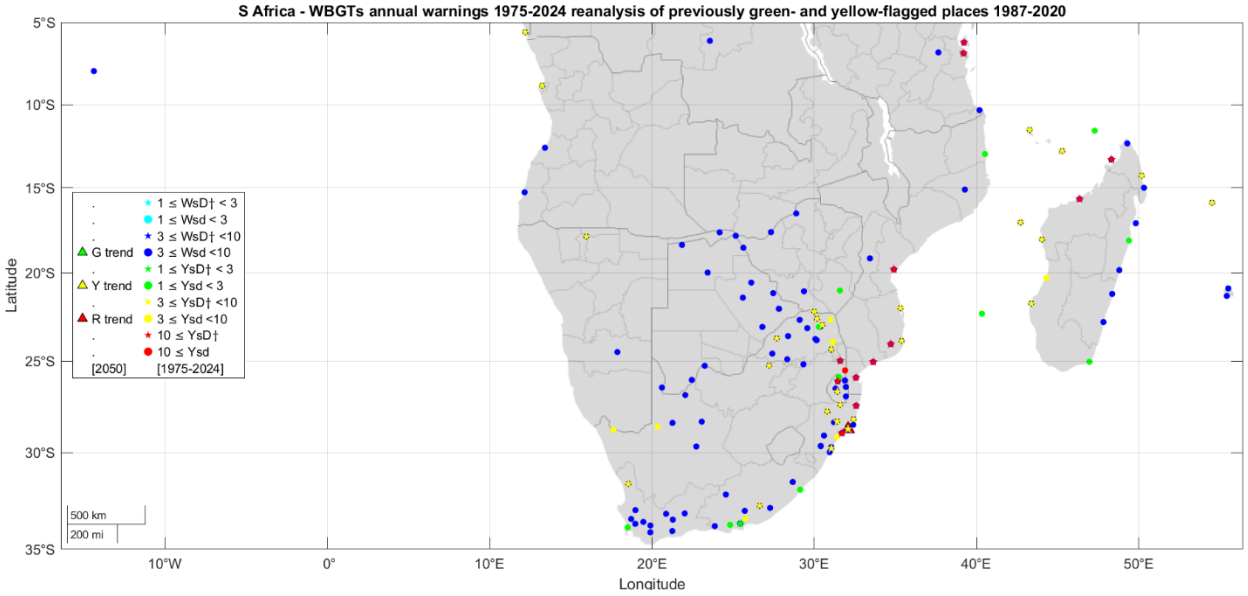

Figure 5: S Africa 1975-2024 reanalysis of previously green-yellow sites and projections

Richards Bay (South Africa) is marked with a red triangle trending (YsD†c2050≥10) based on 113% projection (more than that station's observational history). Above the northern margin there is a West African station, San-Pedro, Côte d'Ivoire that would have been marked with a red triangle and trending with a projection of 93% (being less than that station's observational history).

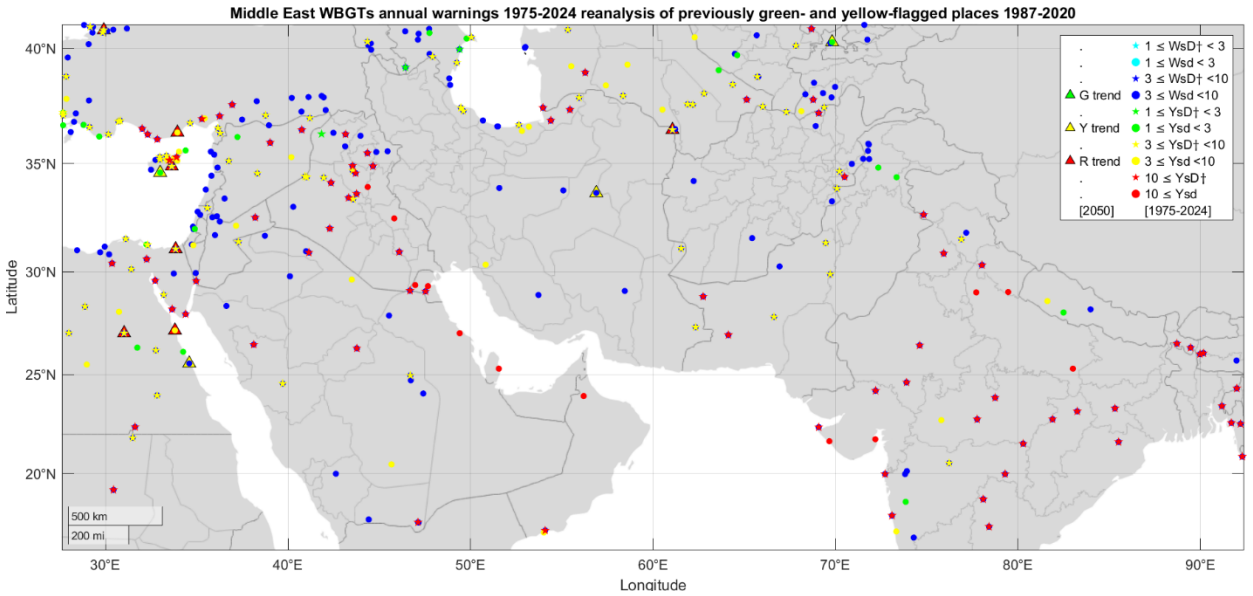

Figure 6: Middle East 1975-2024 reanalysis of previously green-yellow sites and projections

Figure 6 includes Sarakhs Iran, marked with a red (R trend) triangle based on a projection of 135%.

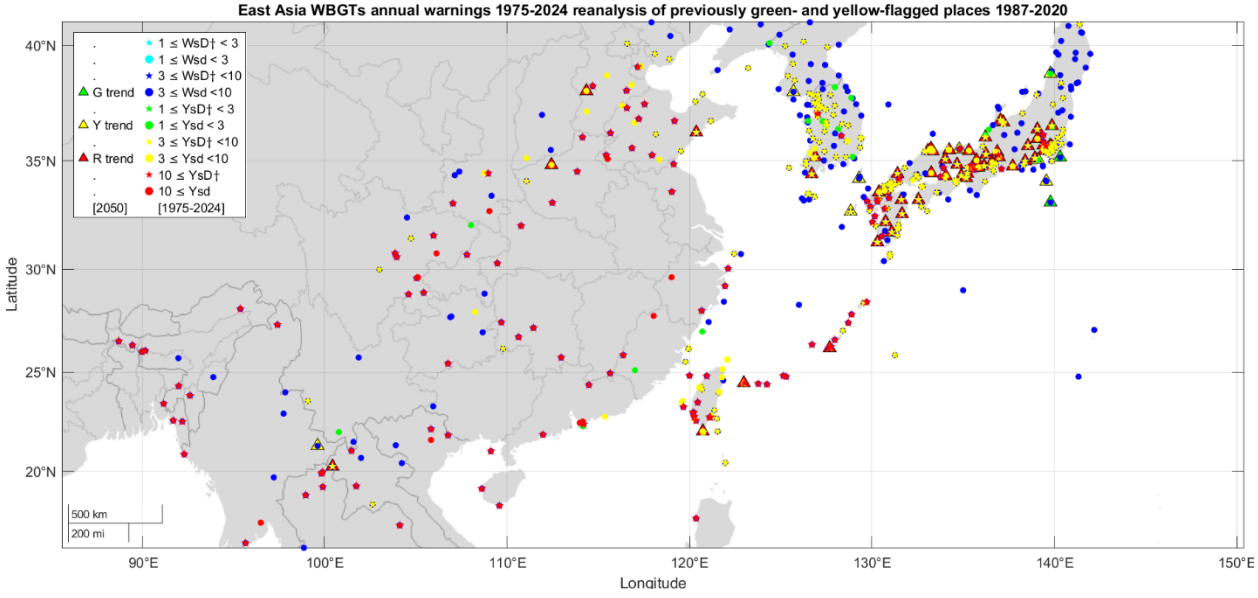

Figure 7: East Asia 1975-2024 reanalysis of previously green-yellow sites and 2050 projections

The 52 locations are marked in Figure 7 with a red triangle (YsD†c2050≥10) are based on projections that are generally less far-fetched than their station histories – with exception of Hengchun Taiwan (235% projection), Tachikawa near Tokyo Japan (235% projection) and Ayase, Kanagawa, Japan (142% projection).

Beyond the eastern frame of Figure 7, Yap would have been marked with a red (R trend) triangle (with reasonably confident 54% projection). Beyond the southern frame there would have been two more red triangles – Klang Dong, Nakhon Ratchasima, Thailand (159% projection) and Seletar Singapore (135% projection).

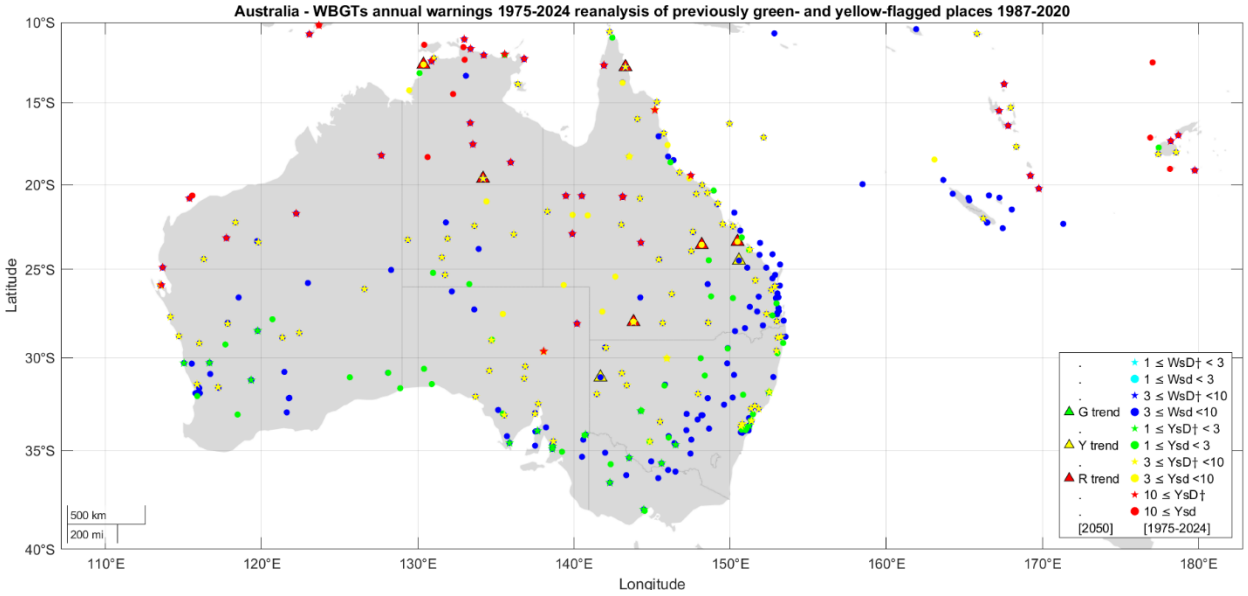

Figure 8: Australia 1975-2024 reanalysis of previously green-yellow sites and projections

Rockhampton, Tennant Creek, Lockhart River, and Emerald are marked with a red triangle trending (YsD†c2050≥10) with projections (60%, 61%, 63%, 77%) that are less than their observational histories, while the red triangle projection at Bynoe Harbour (west of Darwin) is 145% of that station's history, and the projection at Thargomindah (Simpson Desert) is more than 5 times longer than that station's history.

Soekarno Hatta (Jakarta) and Amahai (Maluku) are "green-yellow" locations in Indonesia that missed the map framing but would have been marked with red triangles. Their projections extended only 82% and 90%, so they are not as far-fetched as the duration of their observational histories.

The appendix tabulates projections up to 100% (Table A1) and over 100% (Table A2) trending from the hybrid‡ "green-yellow" classification from 1987-2020 towards the highest risk catagory (5 "red" greater than 10 yellow-flag days in a hot year) by mid-century (YsD†c2050≥10). Note that projections circa year 2050 are based on the observational years (1975-2024) using linear regression slope×2050+intercept+SEE, where SEE is the standard estimate of error of the regression of observations during the period 1975-2024. If these stations where not statistically significantly trended then the slope would be zero, the intercept would be the same as the inter-annual average, and the SEE would be the same as the standard deviation of the interannual variability. But note that these stations were trending such that their green or yellow risk class (3 or 4) during 1987-2020 is projected to transition to red risk class 5 circa 2050. Finally note that such projections are not predictions, but rather suggest the plausibility of future scenarios, and that other locations do not have a long enough history of observations to venture such projections.

Discussion

The current work embarks on reanalysis to extend identification of where public access to air-conditioned shelter may be essential - beyond what was taken from an average exceedance of 10 days per year over the period 1987-2020 (17). The innovation of the present work is applying statistics in hindcasts and projections of the green-yellow cohort of the global network of weather stations where local bioclimatic predilections for rebalancing the heating and cooling

of buildings were previously analysed (48). Meanwhile the current work considers subsequent years through 2024 and further back from 1975 to consider up to a half century of observations. This allows more up-to-date assessment of extreme conditions, and to lay groundwork to leverage the annals to identify non-stationary trends and patterns of changing risk of heat stress through the next quarter century as far as year 2050. Whilst long range forcasting with confidence would require expert use of rapidly evolving hybrids of statistical and machine learning (57, 58), the present work only goes as far as to suggest a prelimary list of locations where there are long enough histories of observations, and then only the cases of smoothly evolving non-stationary climate trends suggesting that air-conditioning may become a necessity circa year 2050.

ISO 7243:2017 (28) Table A.1 only marginally tolerates the "black-flag" threshold (32.2°C WGBT) only up to 32.2°C WGBT for acclimated healthy individuals and only if they are resting and rehydrating. Furthermore, "red-flag" conditions (31.2 - 32.1°C WBGT) preclude productive of unacclimated individuals and severely hinder the capacity of the healthiest adapted cohort. For almost 69 years such "red-flag" conditions have been recognized as an extreme risk during military training (24), requiring rest under shaded shelter soon as practical (19), where "yellow-flag conditions strenuous activities were only manageable with shade". American College of Sports Medicine's recent consensus is to cancel activities in the event of conditions rising above a threshold of 26.8 to 30.1°C WBGT, which depends on local geographic adaptation of athletes (31). This lowering below the long-established lower threshold of "red-flag", tends to support the working assumption that should shaded breezy shelters suffer from more than 10 days reaching "yellow flag" conditions (29.5 - 31.1°C WBGT) then it is essential that cooler shelter be provided for all, while more vulnerable individuals may require cool relief at lower thresholds.

The threat of electricity grid power blackouts during heat waves recommends that rooftop photovoltaic powered air-conditioning (59, 60) should be considered during the design of such

shelters. Otherwise blackouts amplify morbidity and mortality in communities that depend on air-conditioning (9).

Suggestions for further research

Local case studies could target locations that are known to be trending with increasing annual yellow-flag days, to apply advanced extreme value statistics to better estimate when and if there will come a time when universal public access to actively-cooled refugia becomes a public health necessity. Other studies should focus on how cooling shelters could be designed to operate off-grid, powered by on-site renewable energy power. Meanwhile, other studies should assess what are acceptable thresholds for exposure for more vulnerable members of local communities, and what measures can be taken to mitigate their individual risk. There also needs to be assessment of the capacity of the local electricity grids to support air-conditioning of vulnerable individuals while encouraging more adapted members of the community to shelter in shaded areas provided with sufficient hydration and ventilation.

Conclusion

Using GSOD (1975–2024) and WBGTs thresholds, I have presented methods to assess where shaded outdoor living areas can serve as refugia from heat waves, and where they might fail. The proposed criteria are that active cooling is necessary for the general population when the shaded wet bulb globe temperature WBGTs $\geq$ 29.5 °C is expected to occur ten days in a hot year (10 YdD†). Under these conditions (10 or more yellow flag days in a single summer) then communities should be advised that passive shade and ventilation are not likely to suffice for adapted healthy individuals, and air-conditioned refugia may be necessary for community health and productivity.

The previously "green-yellow" cohort (risk categories 3–4 during years 1987-2020) was reanalysed with available observations during the half century 1975-2024, which found a

number of statistically significant warming trends, with some stations plausibly expected to become "red" (≥10 YdD†) by year 2050. The dagger notation (†) indicates that this is based on linear trend plus an estimate of interannual-variability. While not predicting future heatwaves, these scenario-based projections may guide proactive monitoring, design and adaptation of public health policies.

In conclusion, air-conditioning is not universally necessary —but may be necessary in locations where shaded WBGTs breaches the "yellow-flag" threshold (29.5°C) ten days in a single hot year. The half-century reanalysis shows a sizable and growing set of such locations worldwide. Policy and design should focus on access to actively-cooled refugia backed up by on-site solar PV generation in hot climates, while also promoting passive and low-energy measures to limit electricity grid overloads and to provide resilience during blackouts in temperate climates. Local electricity grids should be maintained so that elders and other vulnerable individuals who are house-bound to be able to use air-conditioning – while others are able to take comfort in outdoor shaded refugia such as parks and gardens endowed with shade trees.

Acknowledgments

- unfunded
- No conflicts of interest

References

1. Barreca A, Clay K, Deschenes O, Greenstone M, Shapiro JS. Adapting to climate change: The remarkable decline in the US temperature-mortality relationship over the twentieth century. Journal of Political Economy. 2016;124(1):105-59.
2. Arsenault R. The end of the long hot summer: The air conditioner and southern culture. The Journal of Southern History. 1984;50(4):597-628.

3. Carrier WH. The Economics of Man-Made Weather. Scientific American. 1933;148(4):199-202.

4. Foruzanmehr A, Vellinga M. Vernacular architecture: questions of comfort and practicability. Building Research & Information. 2011;39(3):274-85.

5. Pan Y, Zhong W, Zheng X, Xu H, Zhang T. Natural ventilation in vernacular architecture: A systematic review of bioclimatic ventilation design and its performance evaluation. Building and Environment. 2024;253:111317.

6. Givoni B. Comfort, climate analysis and building design guidelines. Energy and buildings. 1992;18(1):11-23.

7. Camara T, Kamsu-Foguem B, Diourte B, Maiga AI, Habbadi A. Management and assessment of performance risks for bioclimatic buildings. Journal of Cleaner Production. 2017;147:654-67.

8. Winter T. An uncomfortable truth: air-conditioning and sustainability in Asia. Environment and Planning A. 2013;45(3):517-31.

9. Stone Jr B, Gronlund CJ, Mallen E, Hondula D, O'Neill MS, Rajput M, et al. How blackouts during heat waves amplify mortality and morbidity risk. Environmental Science & Technology. 2023;57(22):8245-55.

10. QDC QDC. 6-star energy standard for houses and townhouses | Business Queensland Brisbane, Australia: Queensland Government; 2023 [updated 19 September 2023. Available from: https://www.business.qld.gov.au/industries/building-property-development/building-construction/laws-codes-standards/sustainable-housing/energy-equivalence/6-star.

11. O'Leary T, Belusko M, Whaley D, Bruno F. Comparing the energy performance of Australian houses using NatHERS modelling against measured household energy consumption for heating and cooling. Energy and Buildings. 2016;119:173-82.

12. Williamson T, Damiati SA, Soebarto V, editors. Developing a methodology to assess potential overheating of houses in Darwin. International Conference on the Architectural

Science Association; 2022; Perth, Australia: The Architectural Science Association and Curtin University.

13. Mulville M, Harrington S, Li C, Raushan K, Essien-Thompson E, Ahern C. Dwelling overheating in risk in cool climates: Assessing the risk in the context of retrofit and climate change in Ireland. Indoor Environments. 2025;2(1):100072.

14. Thomas MJ, editor Inside outside: A relationship that moves me. 40th Annual ANZAScA Conference; 2006.

15. Daniel L. 'We like to live in the weather': cooling practices in naturally ventilated dwellings in Darwin, Australia. Energy and Buildings. 2018;158:549-57.

16. Zhang C, Kazanci OB, Levinson R, Heiselberg P, Olesen BW, Chiesa G, et al. Resilient cooling strategies–A critical review and qualitative assessment. Energy and Buildings. 2021;251:111312.

17. Peterson EL. Global and local bioclimatic predilections for rebalancing the heating and cooling of buildings. Energy and Buildings. 2022;266:112088.

18. Peterson E. Transition Engineering the water-electricity nexus operating in building services and urban heat islands – Concept Design – is air-conditioning really necessary? ASHRAE 3rd International Conference on Efficient Building Design; American University, Beirut.: ASHRAE; 2018.

19. Budd GM. Wet-bulb globe temperature (WBGT)—its history and its limitations. Journal of Science and Medicine in Sport. 2008;11(1):20-32.

20. Sullivan JM. Heat Illness In The Emergency Department: Keeping Your Cool. 2014.

21. Cheung HK, Levermore GJ, Watkins R. A low cost, easily fabricated radiation shield for temperature measurements to monitor dry bulb air temperature in built up urban areas. Building Services Engineering Research and Technology. 2010;31(4):371-80.

22. Liljegren JC, Carhart RA, Lawday P, Tschopp S, Sharp R. Modeling the wet bulb globe temperature using standard meteorological measurements. Journal of occupational and environmental hygiene. 2008;5(10):645-55.

23. ASHRAE ASoH, Refrigeration and Air Conditioning Engineers. Chapter 1–Psychrometrics, . ASHRAE Handbook of Fundamentals. Atlanta, Georgia, USA: ASHRAE; 2009.

24. Minard D, Belding HS, Kingston JR. Prevention of heat casualties. Journal of the American Medical Association. 1957;165(14):1813-8.

25. Tartarini F, Schiavon S, Cheung T, Hoyt T. CBE Thermal Comfort Tool: Online tool for thermal comfort calculations and visualizations. SoftwareX. 2020;12:100563.

26. ISO IOfS. ISO 7730 Ergonomics of the Thermal Environment-Analytical Determination and Interpretation of Thermal Comfort Using Calculation of the PMV and PPD Indices and Local Thermal Comfort Criteria. International Organization for Standardization; 2005.

27. Meng X, Meng L, Gao Y, Li H. A comprehensive review on the spray cooling system employed to improve the summer thermal environment: application efficiency, impact factors, and performance improvement. Building and Environment. 2022;217:109065.

28. ISO IOfS. 7243: Ergonomics of the thermal environment—assessment of heat stress using the wbgt (wet bulb globe temperature) index. Int Org Standard Geneva Switzerland. 2017.

29. Wilson A. Passive survivability. Understanding and Quantifying the Thermal Habitability of Buildings during Power Outages. In: Rajkovich NB, Holmes SH, editors. Climate Adaptation and Resilience Across Scales: From Buildings to Cities. New York: Routledge; 2021. p. 141-52.

30. Yaglou C, Minaed D. Control of heat casualties at military training centers. 1957.

31. Roberts WO, Armstrong LE, Sawka MN, Yeargin SW, Heled Y, O'Connor FG. ACSM expert consensus statement on exertional heat illness: recognition, management, and return to activity. Current Sports Medicine Reports. 2023;22(4):134-49.

32. Armstrong LE, Casa DJ, Millard-Stafford M, Moran DS, Pyne SW, Roberts WO. Exertional heat illness during training and competition. Medicine & Science in Sports & Exercise. 2007;39(3):556-72.

33. Jendritzky G, De Dear R, Havenith G. UTCI—why another thermal index? International journal of biometeorology. 2012;56(3):421-8.

34. Havenith G, Fiala D. Thermal indices and thermophysiological modeling for heat stress. Comprehensive physiology. 2011;6(1):255-302.

35. Bröde P, Fiala D, Błażejczyk K, Holmér I, Jendritzky G, Kampmann B, et al. Deriving the operational procedure for the Universal Thermal Climate Index (UTCI). International journal of biometeorology. 2012;56(3):481-94.

36. Havenith G, Smallcombe JW, Hodder S, Jay O, Foster J. Comparing the efficacy of different climate indices for prediction of labor loss, body temperatures, and thermal perception in a wide variety of warm and hot climates. Journal of Applied Physiology. 2024;137(2):312-28.

37. Kjellstrom T, Lemke B, Briggs D, Otto M, Hasson L. Climate Change Heat Impact & Prevention | Climate CHIP Mapua, Nelson, New Zealand: Health and Environment International Trust (HEIT); 2025 [updated November 25, 2025. Available from: https://www.climatechip.org/.

38. Otto M, Lemke B, Kjellstrom T. Hothaps-Soft: A tool for the estimation and analysis of local climate and population heat exposure. Nelson, New Zealand: Climate Change Health Impact & Prevention; 2014. Contract No.: Technical report 2014: 3.

39. Betti G, Tartarini F, Nguyen C, Schiavon S, editors. CBE Clima Tool: A free and open-source web application for climate analysis tailored to sustainable building design. Building Simulation; 2024: Springer.

40. Wang W, Li S, Guo S, Ma M, Feng S, Bao L. Benchmarking urban local weather with long-term monitoring compared with weather datasets from climate station and EnergyPlus weather (EPW) data. Energy Reports. 2021;7:6501-14.

41. Herb S, Wolk S, Reinhart C. Beyond the bioclimatic chart: An automated simulation-based method for the assessment of natural ventilation and passive design potential. Building and Environment. 2025;269:112362.

42. Kjellstrom T, Lemke B, Otto M. Mapping occupational heat exposure and effects in South-East Asia: ongoing time trends 1980–2011 and future estimates to 2050. Industrial health. 2013;51(1):56-67.

43. Peterson E, editor Transition Engineering the Water-Electricity Nexus Operating in Building Services and Urban Heat Islands – Concept Design - Is Air-Conditioning Really Necessary? The Third International Conference on Efficient Building Design; 2018; American University Beirut, Lebanon: ASHRAE.

44. Peterson EL. Where air-conditioning is essential: weather station analysis of limits for passive cooling. CIBSE Technical Symposium 2026 - Fit for 2050 - Redesigning Spaces for Wellbeing, Inclusivity, and Sustainable Performance; Loughborough University, 26 - 27 March, 2026. London: CIBSE; 2026.

45. NCEI NCfEI. Global Hourly - Integrated Surface Database (ISD) | National Centers for Environmental Information (NCEI) National Climatic Data Center, 151 Patton Avenue, Asheville, NC 28801 USA: NOAA's National Centers for Environmental Information; 2024 [Available from: https://www.ncei.noaa.gov/products/land-based-station/integrated-surface-database.

46. Smith A, Lott N, Vose R. The integrated surface database: Recent developments and partnerships. Bulletin of the American Meteorological Society. 2011;92(6):704-8.

47. NCEI NCfEI. Global Surface Summary of Day Data (GSOD) Asheville, NC 28801 USA, www.ncei.noaa.gov NOAA's National Centers for Environmental Information (NCEI), Center for Weather and Climate (CWC); 2020 [updated July 2025. Available from: https://www.ncei.noaa.gov/data/global-summary-of-the-day/.

48. Peterson E. Data associated with "Global and local bioclimatic predilections for rebalancing the heating and cooling of buildings". [Dataset]. . In: Visiting Research Fellow SoB, University of Leeds, editor. Leeds, West Yorkshire, United Kingdom2022.

49. Kuhnel I, Coates L. El Niño-Southern Oscillation: related probabilities of fatalities from natural perils in Australia. Natural Hazards. 2000;22(2):117-38.

50. Wickham FA. Air Conditioning Systems: Load Estimation & Associated Psychrometrics. 2nd ed: Australian Government Publishing Service; 1988.

51. Peterson E. predilection | CC (country code FIPS country codes link to summary of stations and their psychrometric charts) 2022 [Available from: https://bioclimatic.github.io/CC/.

52. Burkey J. Mann-Kendall Tau-b with Sen's Method (enhanced). Version 1.15.0.2 ed. Mathworks: King County, Department of Natural Resources and Parks, Science and Technical Services section, Seattle, Washington, USA; 2020.

53. Kjellstrom T, Freyberg C, Lemke B, Otto M, Briggs D. Estimating population heat exposure and impacts on working people in conjunction with climate change. International journal of biometeorology. 2018;62(3):291-306.

54. Mora C, Dousset B, Caldwell IR, Powell FE, Geronimo RC, Bielecki CR, et al. Global risk of deadly heat. Nature Climate Change. 2017;7(7):501-6.

55. WorldPop. The spatial distribution of population in 2020. In: WorldPop (www.worldpop.org - School of Geography and Environmental Science UoSDoGaG, University of Louisville; Departement de Geographie, Universite de Namur) and Center for International Earth Science Information Network (CIESIN), Columbia University (2018). , editor. Global High Resolution Population Denominators Project - Funded by The Bill and Melinda Gates Foundation (OPP1134076) 2019.

56. Center for International Earth Science Information Network - CIESIN - Columbia University. Gridded Population of the World, Version 4 (GPWv4): Population Density, Revision 11. Palisades, NY: NASA Socioeconomic Data and Applications Center (SEDAC); 2018.

57. Olukoya O. Time series-based quantitative risk models: enhancing accuracy in forecasting and risk assessment. International Journal of Computer Applications Technology and Research. 2023;12(11):29-41.

58. Kaya Y. Slope-aware and self-adaptive forecasting of water levels: A transparent model for the Great Lakes under climate variability. Journal of Hydrology. 2025:133948.

59. Rogers T, Al-Habaibeh A, Donastorg Sosa A, Vahidinasab V. Rising temperatures mean more air conditioning which means more electricity is needed–rooftop solar is a perfect fit. The Conversation. 2023.

60. Bakhshi-Jafarabadi R, Seyed Mousavi SM. Peak load shaving of air conditioning loads via rooftop grid-connected photovoltaic systems: a case study. Sustainability. 2024;16(13):5640.

Appendix Table A1: Projections up to 100% trending from green-yellow towards red by mid-century ($YsD\dagger_{c2050} \geq 10$)

USAF	WBAN	STATIONNAME	LAT	LON	base	stop	WsD†	YsD†	$risk_{c2024}$	project	$risk_{c2050}$	$WsD\dagger_{c2050}$	$YsD\dagger_{c2050}$
722630	23034	SAN ANGELO	31.352	-100.5	1975	2024	128	8	4	54%	5	150	11
723530	13967	WILL ROGERS AP	35.388	-97.6	1975	2024	91	9	4	54%	5	103	11
722120	12833	CROSS CITY AP	29.633	-83.11	1978	2023	143	9	4	64%	5	196	15
782440	99999	JAIME GONZALEZ	22.15	-80.41	2002	2024	244	8	4	77%	5	366	29
724520	3957	MEDICINE LDG	37.284	-98.55	1984	2024	76	7	4	79%	5	96	11
872220	99999	CATAMARCA	-28.6	-65.75	1975	2024	101	9	4	54%	5	115	12
786390	99999	RETALHULEU	14.521	-91.7	2008	2024	356	4	4	71%	5	366	17
787410	99999	MANAGUA	12.141	-86.17	1975	2024	355	9	4	73%	5	366	15
917590	99999	FALEOLO INTL	-13.83	-172	1998	2024	363	8	4	82%	5	366	25
787390	99999	CHINANDEGA	12.633	-87.13	1976	2024	349	9	4	90%	5	366	19
873200	99999	CHAMICAL AERO	-30.37	-66.28	1976	2022	78	9	4	94%	5	93	13
861920	99999	SAN ESTANISLAO	-24.67	-56.46	2000	2023	151	8	4	97%	5		30
872440	99999	VILLA MARIA RIO	-29.9	-63.68	1977	2024	67	6	4	100%	5	100	11
917540	99999	POINTE VELE	-14.31	-178.1	1982	2021	327	5	4	100%	5	366	11
163320	99999	LECCE	40.239	18.133	1975	2024	76	9	4	54%	5	99	13
166060	99999	SERRAI	41.067	23.567	2015	2024	56	2	3	56%	5		15

605900	99999	EL GOLEA	30.571	2.86	1975	2024	118	9	4	57%	5	142	12
176090	99999	LARNAKA INTL	34.875	33.625	1978	2024	108	8	4	57%	5	143	11
173300	99999	SILIFKE	36.383	33.933	1975	2024	107	9	4	57%	5	131	12
607480	99999	SIDI BOUZID	35	9.483	1979	2024	96	9	4	61%	5	124	12
136110	99999	DURRES	41.3	19.45	1987	2024	66	8	4	68%	5	131	18
623930	99999	ASYUT INTL	27.047	31.012	1982	2024	140	8	4	71%	5	199	11
163340	99999	OTRANTO	40.1	18.483	2006	2021	69	5	4	75%	5	228	23
162320	99999	TERMOLI	42	15	1989	2024	62	7	4	79%	5	123	18
624630	99999	HURGHADA INTL	27.178	33.799	1991	2024	138	9	4	79%	5	170	16
165390	99999	CAPE FRASCA	39.75	8.467	1975	2021	65	7	4	81%	5		10
623370	99999	EL ARISH INTL	31.073	33.836	1986	2024	100	6	4	87%	5	152	15
655940	99999	SAN PEDRO	4.747	-6.661	1979	2024	333	9	4	93%	5	366	15
914130	40308	YAP AIRPORT	9.483	138.08	1975	2024	377	7	4	54%	5	366	12
USAF	WBAN	STATIONNAME	LAT	LON	base	stop	WsD†	YsD†	$risk_{c2024}$	project	$risk_{c2050}$	$WsD†_{c2050}$	$YsD†_{c2050}$
479360	99999	NAHA	26.2	127.68	1975	2024	149	9	4	54%	5	162	12
478150	99999	OITA	33.233	131.62	1975	2024	81	7	4	54%	5	91	10
478070	99999	FUKUOKA	33.583	130.38	1975	2024	74	8	4	54%	5	92	18
478910	99999	TAKAMATSU	34.317	134.05	1975	2024	74	7	4	54%	5	95	15

477720	99999	OSAKA	34.683	135.52	1975	2024	74	7	4	54%	5	88	14
471560	99999	GWANGJU	35.167	126.9	1975	2024	68	9	4	54%	5	77	12
476360	99999	NAGOYA	35.167	136.97	1975	2024	70	8	4	54%	5	92	17
476340	99999	GIFU	35.394	136.87	1975	2024	74	9	4	54%	5	85	12
477410	99999	MATSUE	35.45	133.07	1975	2024	64	5	4	54%	5	84	10
477460	99999	TOTTORI	35.483	134.23	1975	2024	66	7	4	54%	5	87	16
476620	99999	TOKYO	35.683	139.77	1975	2024	64	6	4	54%	5	89	13
548570	99999	LIUTING	36.266	120.37	1975	2024	66	8	4	54%	5	86	12
476240	99999	MAEBASHI	36.4	139.07	1975	2024	57	5	4	54%	5	80	11
536980	99999	SHIJIAZHUANG	38.067	114.35	1975	2024	68	9	4	54%	5	76	11
477500	99999	MAIZURU	35.45	135.32	1975	2024	66	8	4	55%	5	90	19
476380	99999	KOFU	35.667	138.55	1975	2024	61	6	4	55%	5	84	14
477770	99999	WAKAYAMA	34.233	135.17	1976	2024	71	5	4	57%	5	85	11
476150	99999	UTSUNOMIYA	36.55	139.87	1976	2024	54	5	4	57%	5	80	11
477590	99999	KYOTO	35.017	135.73	1976	2024	67	8	4	59%	5	88	17
476070	99999	TOYAMA	36.717	137.2	1976	2024	57	6	4	59%	5	82	13
471700	99999	WANDO	34.4	126.7	1984	2024	66	8	4	66%	5	86	12
570710	99999	MENGJIN	34.817	112.43	1984	2024	64	9	4	66%	5	75	14

489260	99999	HOUEI-SAI *	20.25	100.43	2011	2023	222	8	4	72%	5	343	39
476870	99999	TOKYO HELIPORT	35.633	139.85	1989	2024	63	5	4	75%	5	98	14
476410	99999	CHICHIBU	35.983	139.07	1992	2024	56	7	4	75%	5	76	16
476160	99999	FUKUI	36.05	136.22	1992	2024	64	5	4	75%	5	93	13
476840	99999	YOKKAICHI	34.933	136.58	1992	2024	67	8	4	77%	5	91	19
476560	99999	SHIZUOKA	34.983	138.4	1992	2024	70	6	4	77%	5	92	15
476570	99999	MISHIMA	35.117	138.93	1992	2024	69	6	4	77%	5	93	15
476540	99999	HAMAMATSU	34.75	137.72	1992	2024	73	8	4	79%	5	99	21
476490	99999	UENO	34.767	136.15	1992	2024	67	5	4	79%	5	90	13
USAF	WBAN	STATIONNAME	LAT	LON	base	stop	WsD†	YsD†	$risk_{c2024}$	project	$risk_{c2050}$	$WsD†_{c2050}$	$YsD†_{c2050}$
477610	99999	HIKONE	35.283	136.25	1993	2024	64	6	4	79%	5	88	16
476060	99999	FUSHIKI	36.8	137.05	1992	2024	55	5	4	79%	5	83	13
478240	99999	HITOYOSHI	32.217	130.75	1993	2024	80	7	4	82%	5	99	19
477440	99999	YONAGO	35.433	133.33	1993	2024	63	7	4	82%	5	86	18
477540	99999	HAGI	34.417	131.4	1993	2024	67	6	4	84%	5	86	15
477800	99999	NARA	34.7	135.83	1993	2024	68	7	4	84%	5	91	17
479110	99999	YONAGUNI	24.467	122.98	1991	2024	149	7	4	87%	5	196	31
478290	99999	MIYAKONOJO	31.733	131.08	1993	2024	81	4	4	87%	5		11

478920	99999	UWAJIMA	33.233	132.55	1993	2024	78	6	4	87%	5		14
478090	99999	IIZUKA	33.65	130.7	1993	2024	73	9	4	87%	5		23
477760	99999	SUMOTO	34.333	134.9	1995	2024	64	6	4	87%	5	89	19
477690	99999	HIMEJI	34.833	134.67	1995	2024	67	6	4	87%	5		17
477420	99999	SAKAI	35.55	133.23	1995	2024	62	6	4	87%	5		16
478310	99999	MAKURAZAKI	31.267	130.3	1995	2024	87	7	4	90%	5		20
477670	99999	FUKUYAMA	34.45	133.25	1995	2024	70	8	4	90%	5		25
478220	99999	NOBEOKA	32.583	131.65	1995	2024	79	4	4	93%	5		12
477740	99999	KANSAI INTL	34.433	135.23	1996	2024	72	7	4	93%	5		12
477560	99999	TSUYAMA	35.067	134.02	1994	2024	63	6	4	93%	5		18
943740	99999	ROCKHAMPTON	-23.38	150.48	1975	2024	102	7	4	60%	5	141	12
942380	99999	TENNANT CREEK	-19.63	134.18	1975	2024	131	7	4	61%	5	159	11
941860	99999	LOCKHART RIVER	-12.78	143.3	1976	2024	226	6	4	63%	5	324	10
943630	99999	EMERALD	-23.57	148.18	1989	2024	128	8	4	77%	5	159	11
967490	99999	SOEKARNOHATTA	-6.126	106.66	1988	2024	368	6	4	82%	5		13
977220	99999	AMAHAI	-3.35	128.88	1995	2024	343	8	4	90%	5	366	17

Appendix Table A2: Far-fetched projections (over 100%) trending from green-yellow towards red by mid-century ($YsD\dagger_{c2050} \geq 10$)

USAF	WBAN	STATIONNAME	LAT	LON	base	stop	WsD†	YsD†	$risk_{c2024}$	project	$risk_{c2050}$	$WsD\dagger_{c2050}$	$YsD\dagger_{c2050}$
722220	99999	PENSACOLA FL	30.483	-87.18	2005	2024	110	4	4	123%	5		11
722320	12884	BATON ROUGE	29.333	-89.41	1975	2010	137	9	4	128%	5	172	30
720354	63901	ALTUS	34.699	-99.34	2006	2024	99	9	4	142%	5		15
746140	23112	NELLIS AFB	36.25	-115	2006	2024	61	4	4	142%	5		11
722103	12895	ST LUCIE COUNTY	27.498	-80.38	2007	2024	184	8	4	150%	5	227	15
722537	12961	KRVL AP	29.983	-99.08	2007	2024	129	5	4	150%	5	180	11
722598	3970	ADDISON AIRPORT	32.969	-96.84	2007	2024	108	8	4	150%	5		16
720305	53964	DECATUR AIRPORT	33.254	-97.58	2007	2024	118	9	4	150%	5	178	21
720261	53976	BRIDGEPORT	33.175	-97.83	2007	2024	105	9	4	159%	5		19
720308	4992	MILLARD AIRPORT	41.196	-96.11	2007	2024	50	6	4	159%	5		11
725484	4942	LE MARS AIRPORT	42.778	-96.19	2007	2024	28	5	4	159%	5		12
720298	53971	CHEROKEECOUNTY	31.869	-95.22	2007	2023	115	9	4	165%	5		20

USAF	WBAN	STATIONNAME	LAT	LON	base	stop	WsD†	YsD†	$risk_{c2024}$	project	$risk_{c2050}$	$WsD†_{c2050}$	$YsD†_{c2050}$
720639	225	HORSESHOE BAY	30.533	-98.37	2010	2024	129	6	4	180%	5		21
747930	12843	VERO BEACH AP	27.655	-80.41	2011	2024	191	9	4	193%	5	255	26
749048	415	KEYSTONE	29.845	-82.05	2012	2024	141	6	4	208%	5		27
720601	193	AIKEN AP	33.65	-81.68	2010	2024	94	2	3	225%	5		12
720924	311	ROSCOE TURNER	34.915	-88.6	2012	2024	88	3	4	225%	5		13
720745	272	BOOMVANGPLATFORM	27.35	-94.63	2011	2024	142	6	4	245%	5		27
720904	299	DELAND MUNICIPAL	29.067	-81.28	2014	2024	149	3	4	245%	5		17
721048	471	PRESIDIO LELY AIRPORT	29.634	-104.4	2014	2024	97	3	4	245%	5		18
720169	116	WASHINGTON AIRPORT	38.583	-91	2013	2024	64	7	4	245%	5		35
722673	99999	SHERMAN-DENISON	33.72	-96.67	1984	2002	96	6	4	258%	5		17
721042	486	ZEPHYRHILLS	28.228	-82.16	2013	2024	164	7	4	270%	5		31
722115	99999	SARASOTA BRADENTON	27.383	-82.55	1975	1997	173	8	4	300%	5	243	20
724509	99999	NEWTON CITY CO	38.058	-97.27	1993	2005	56	3	4	354%	5	213	15
720141	4868	MARSHALL CO	41.019	-89.39	2007	2012	49	2	3	650%	5		28

787950	99999	RUBEN CANTU	8.086	-80.95	1981	2021	349	8	4	120%	5		15
862100	99999	SALTOS DEL GUAIRA	-24.03	-54.35	1997	2024	144	7	4	150%	5		17
789700	99999	PIARCO	10.595	-61.34	1975	2004	386	7	4	157%	5	366	14
801440	99999	EL CARANO	5.691	-76.64	2010	2024	365	9	4	169%	5	366	37
804480	99999	GUASDUALITO	7.211	-70.76	1983	2015	371	9	4	189%	5	366	24
788060	99999	HOWARD	8.917	-79.6	1975	2002	363	3	4	233%	5	366	10
789510	99999	E T JOSHUA	13.144	-61.21	1981	1997	320	3	4	450%	5		15
144430	99999	PALAGRUZA	42.4	16.267	1997	2024	58	7	4	108%	5		11
		RICHARDS BAY											
684950	99999	AIRPORT	-28.73	32.083	2014	2024	99	6	4	113%	5	249	28
607280	99999	NABEUL	36.467	10.7	1983	2023	69	4	4	127%	5	117	10
407809	99999	SARAKHS	36.5	61.067	2005	2024	73	5	4	135%	5	108	11
607310	99999	ENFIDHA	36.083	10.433	2010	2024	87	9	4	180%	5	150	20
167190	99999	ZAKINTHOS	37.783	20.883	2015	2024	66	3	4	193%	5	142	24
622250	99999	TRAGEN	25.933	14.45	2009	2024	82	7	4	225%	5		30
170661	99999	IZMIT	40.767	29.9	2016	2024	62	3	4	300%	5		17
476790	43319	ATSUGI US NAVAL AIR	35.455	139.45	2006	2024	73	6	4	142%	5	109	13
484350	99999	PAKCHONG AGROMET	14.633	101.32	2008	2024	263	9	4	159%	5		26

467520	99999	HENGCHUN	22.041	120.73	1975	1997	193	9	4	235%	5	19
476600	99999	TACHIKAWA (JASDF)	35.7	139.4	1975	1997	52	7	4	235%	5	24
486990	99999	SELETAR	1.417	103.87	2005	2024	358	8	4	135%	5	16
941160	99999	DUM IN MIRRIE	-12.63	130.37	1999	2022	288	8	4	145%	5	16
944920	99999	THARGOMINDAH POST O	-28	143.82	1989	1998	70	5	4	530%	5	40

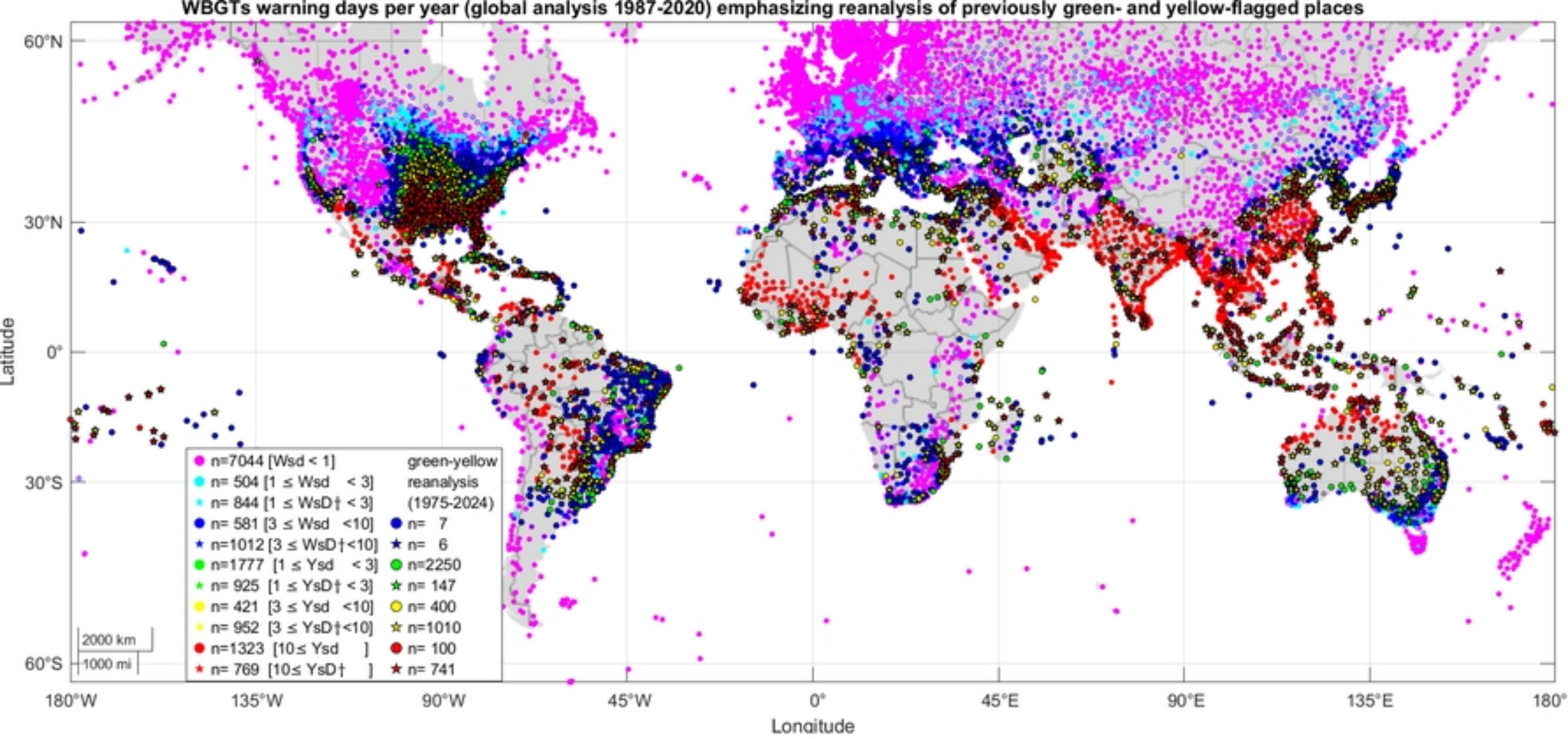
WBGTs warning days per year (global analysis 1987-2020) emphasizing reanalysis of previously green- and yellow-flagged places
60°N
30°N
0°
30°S
60°S
Latitude
180°W
135°W
90°W
45°W
0°
45°E
90°E
135°E
180°
Longitude
n=7044 [Wsd < 1]
n= 504 [1 ≤ Wsd < 3]
n= 844 [1 ≤ WsD† < 3]
n= 581 [3 ≤ Wsd <10]
n=1012 [3 ≤ WsD†<10]
n=1777 [1 ≤ Ysd < 3]
n= 925 [1 ≤ YsD† < 3]
n= 421 [3 ≤ Ysd <10]
n= 952 [3 ≤ YsD†<10]
n=1323 [10≤ Ysd]
n= 769 [10≤ YsD†]
green-yellow reanalysis (1975-2024)
n= 7
n= 6
n=2250
n= 147
n= 400
n=1010
n= 100
n= 741
2000 km
1000 mi

Figure 1

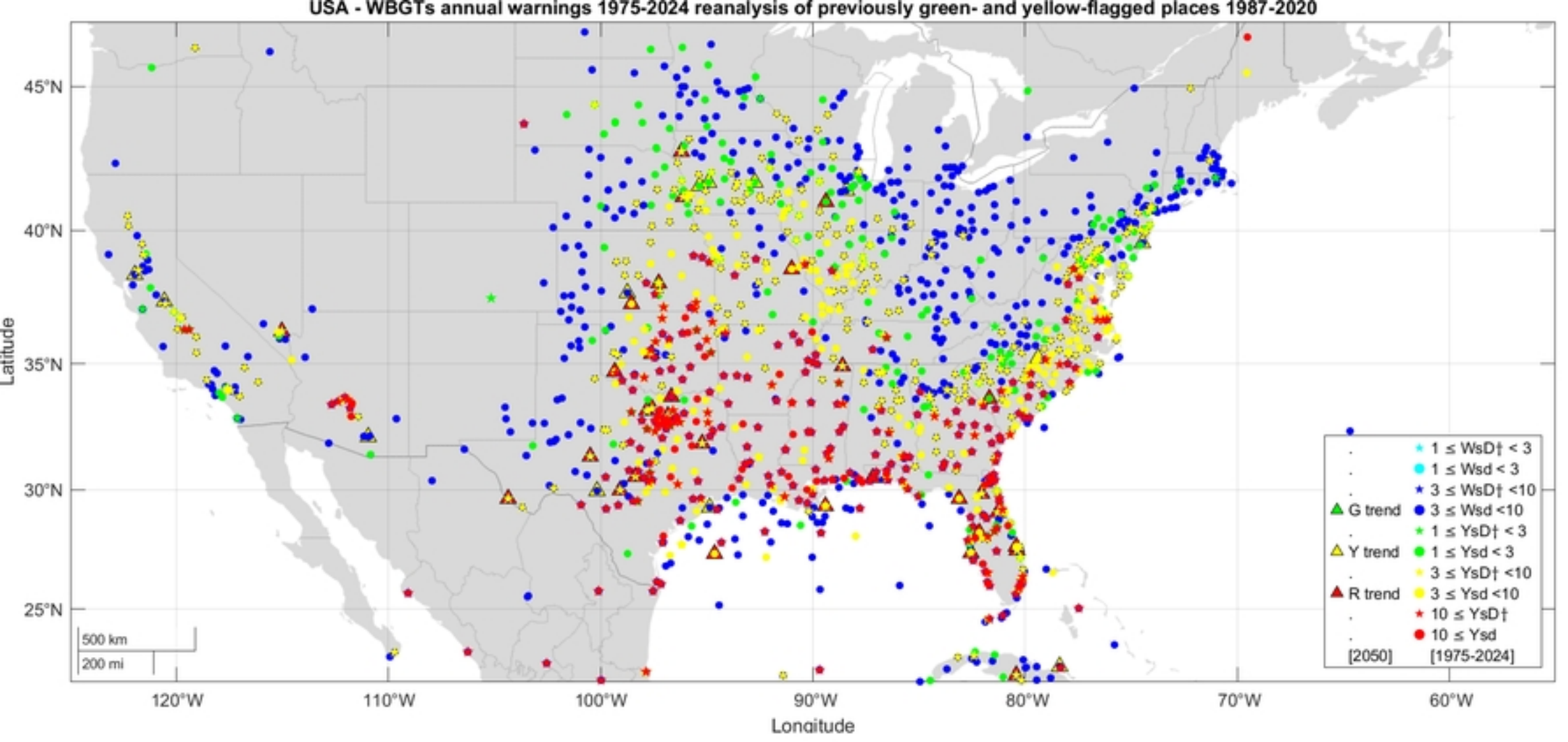
USA - WBGTs annual warnings 1975-2024 reanalysis of previously green- and yellow-flagged places 1987-2020
45°N
40°N
35°N
30°N
25°N
Latitude
120°W
110°W
100°W
90°W
80°W
70°W
60°W
Longitude
500 km
200 mi
G trend
Y trend
R trend
[2050]
1 ≤ WsD† < 3
1 ≤ Wsd < 3
3 ≤ WsD† <10
3 ≤ Wsd <10
1 ≤ YsD† < 3
1 ≤ Ysd < 3
3 ≤ YsD† <10
3 ≤ Ysd <10
10 ≤ YsD†
10 ≤ Ysd
[1975-2024]

Figure 2

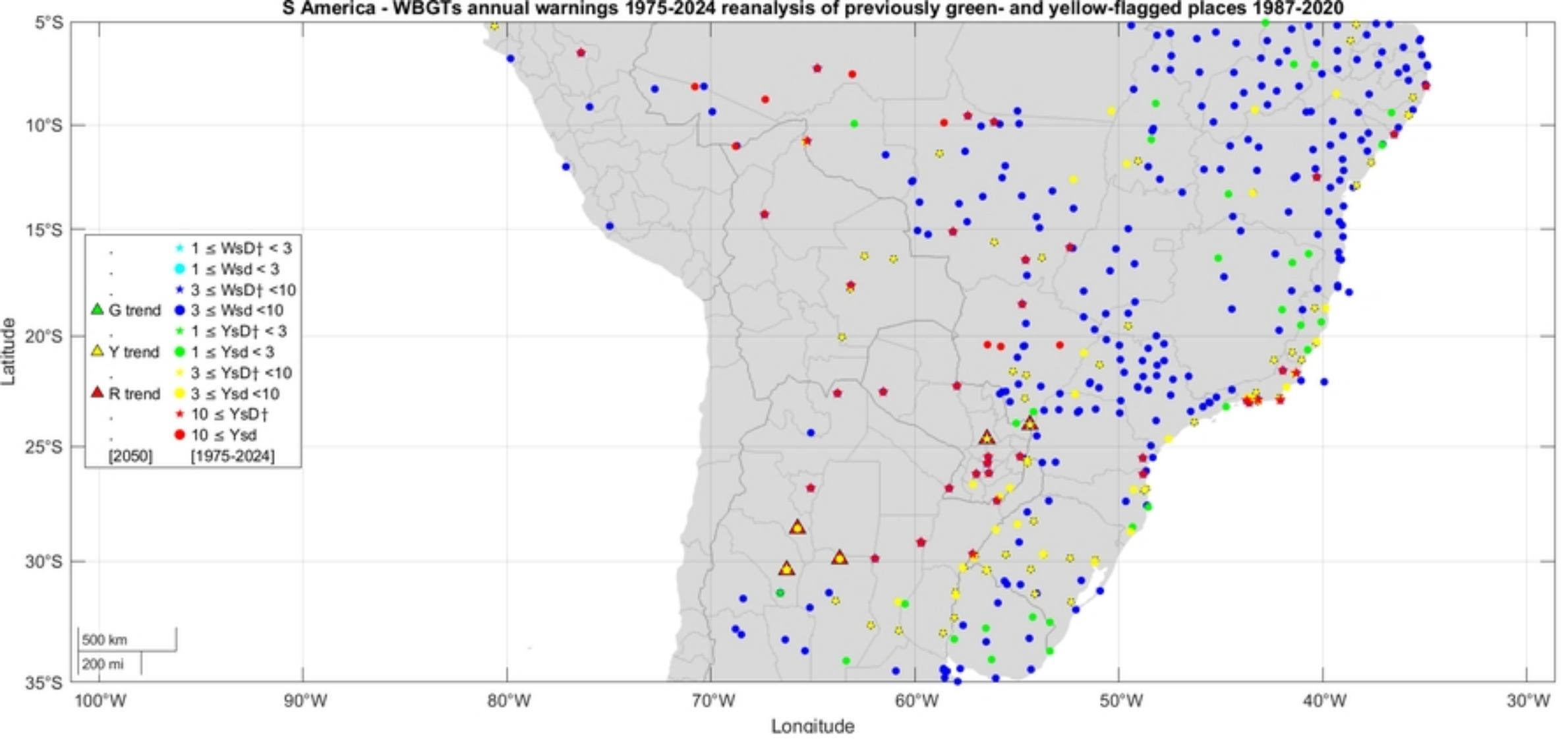
S America - WBGTs annual warnings 1975-2024 reanalysis of previously green- and yellow-flagged places 1987-2020
5°S
10°S
15°S
20°S
25°S
30°S
35°S
Latitude
100°W
90°W
80°W
70°W
60°W
50°W
40°W
30°W
Longitude
G trend
Y trend
R trend
[2050]
1 ≤ WsD† < 3
1 ≤ Wsd < 3
3 ≤ WsD† <10
3 ≤ Wsd <10
1 ≤ YsD† < 3
1 ≤ Ysd < 3
3 ≤ YsD† <10
3 ≤ Ysd <10
10 ≤ YsD†
10 ≤ Ysd
[1975-2024]
500 km
200 mi

Figure 3

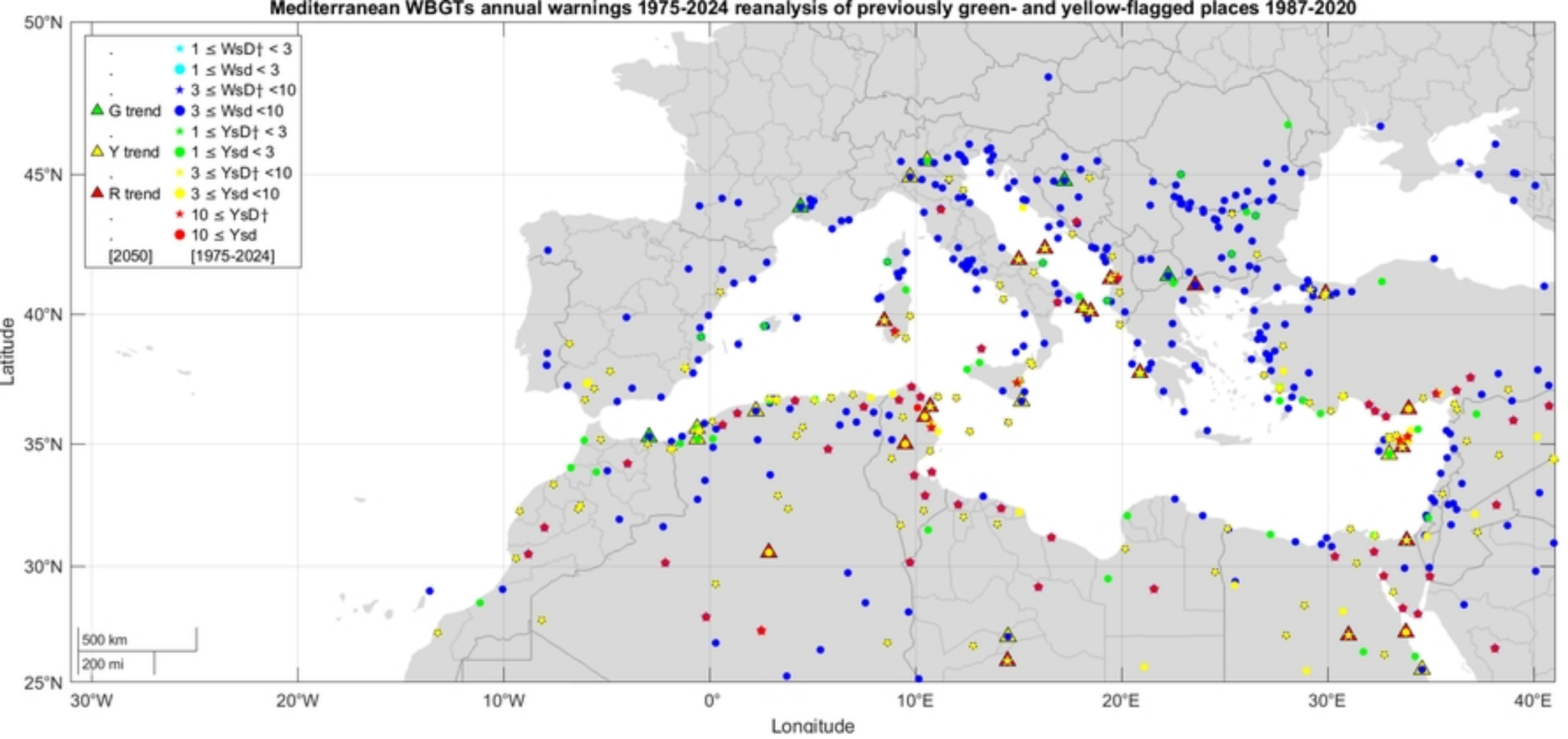
Mediterranean WBGTs annual warnings 1975-2024 reanalysis of previously green- and yellow-flagged places 1987-2020
1 ≤ WsD† < 3
1 ≤ Wsd < 3
3 ≤ WsD† <10
G trend
3 ≤ Wsd <10
1 ≤ YsD† < 3
Y trend
1 ≤ Ysd < 3
3 ≤ YsD† <10
R trend
3 ≤ Ysd <10
10 ≤ YsD†
10 ≤ Ysd
[2050]
[1975-2024]
500 km
200 mi
50°N
45°N
40°N
35°N
30°N
25°N
Latitude
30°W
20°W
10°W
0°
10°E
20°E
30°E
40°E
Longitude

Figure 4

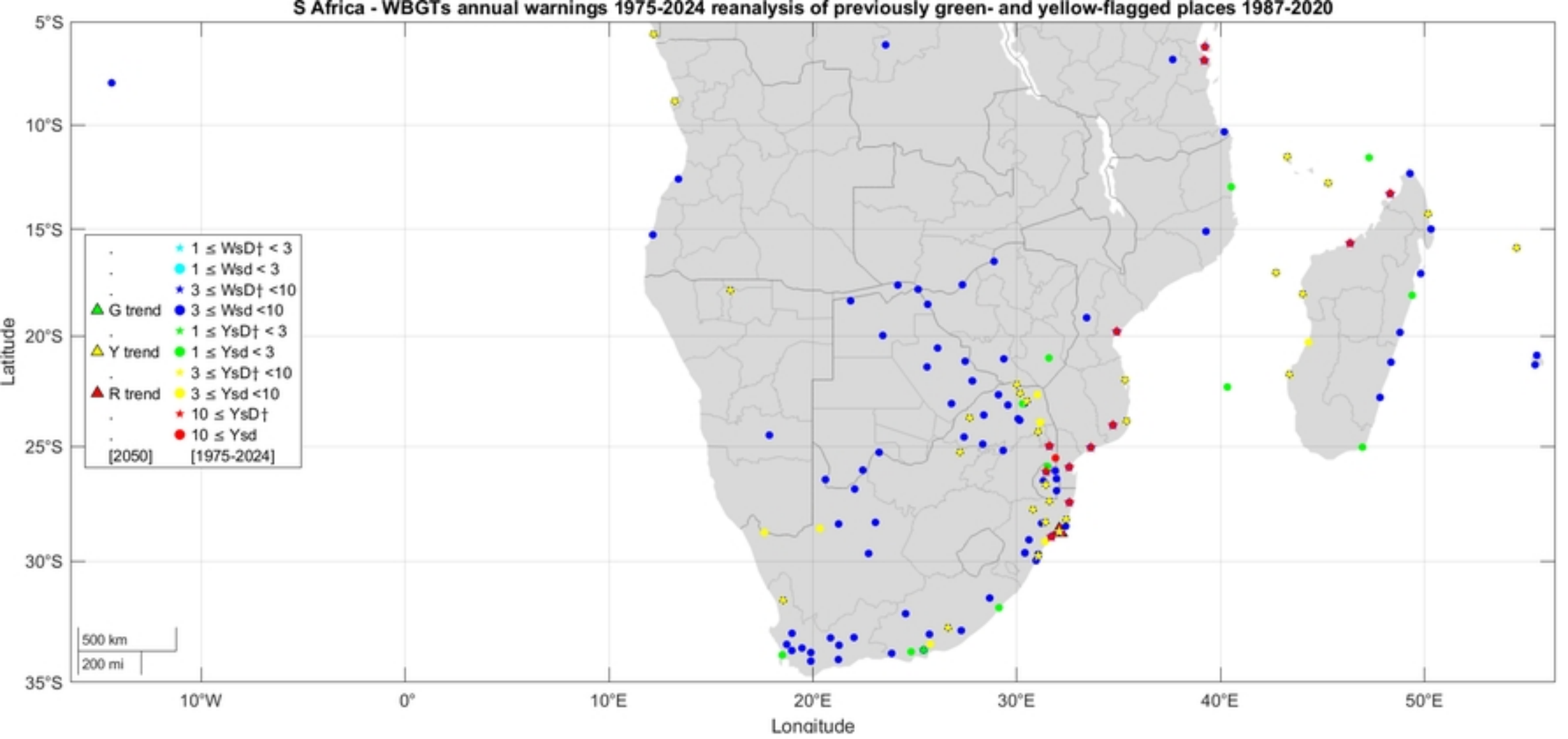
S Africa - WBGTs annual warnings 1975-2024 reanalysis of previously green- and yellow-flagged places 1987-2020
5°S
10°S
15°S
20°S
25°S
30°S
35°S
Latitude
10°W
0°
10°E
20°E
30°E
40°E
50°E
Longitude
G trend
Y trend
R trend
[2050]
1 ≤ WsD† < 3
1 ≤ Wsd < 3
3 ≤ WsD† <10
3 ≤ Wsd <10
1 ≤ YsD† < 3
1 ≤ Ysd < 3
3 ≤ YsD† <10
3 ≤ Ysd <10
10 ≤ YsD†
10 ≤ Ysd
[1975-2024]
500 km
200 mi

Figure 5

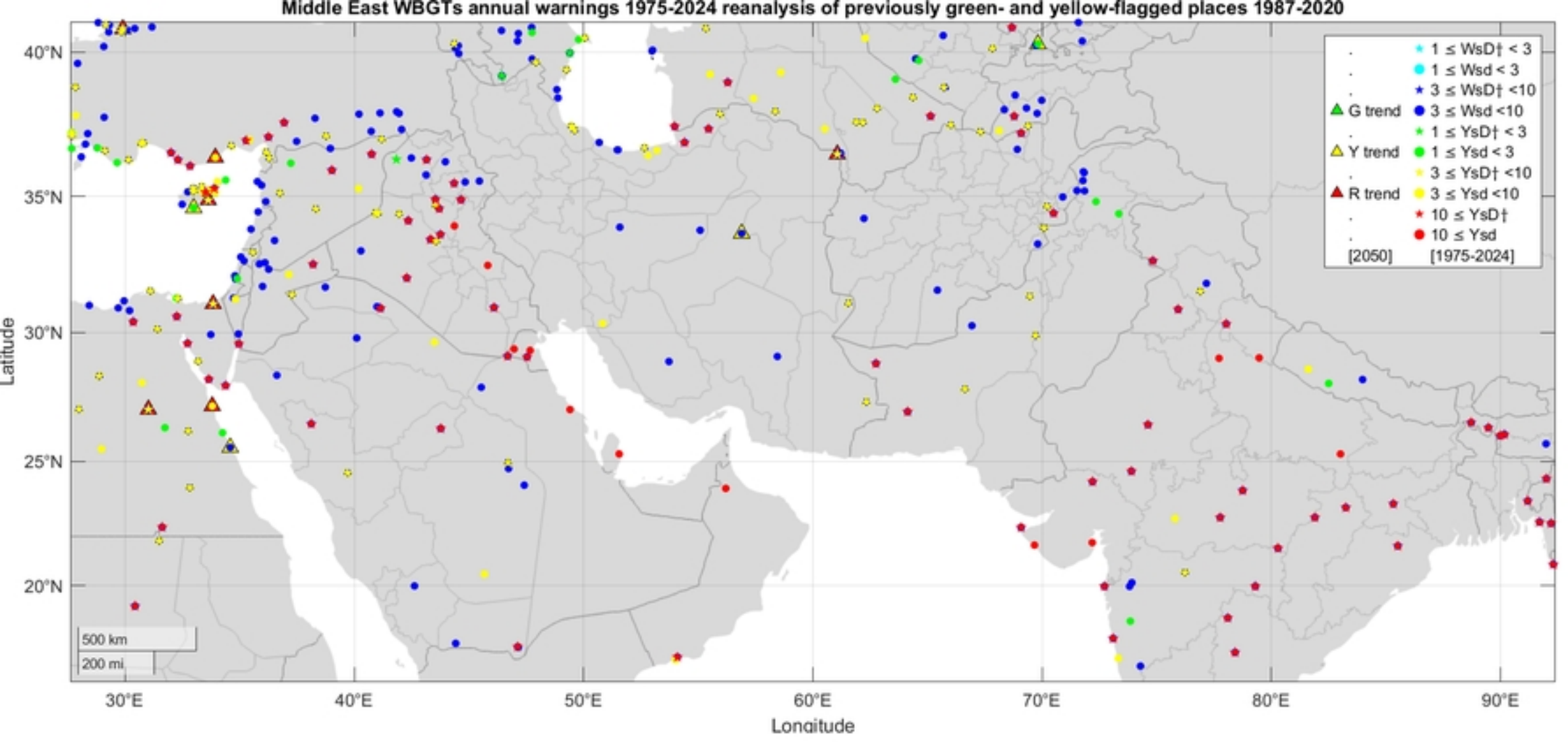
Middle East WBGTs annual warnings 1975-2024 reanalysis of previously green- and yellow-flagged places 1987-2020
40°N
35°N
30°N
25°N
20°N
Latitude
30°E
40°E
50°E
60°E
70°E
80°E
90°E
Longitude
500 km
200 mi
G trend
Y trend
R trend
[2050]
1 ≤ WsD† < 3
1 ≤ Wsd < 3
3 ≤ WsD† <10
3 ≤ Wsd <10
1 ≤ YsD† < 3
1 ≤ Ysd < 3
3 ≤ YsD† <10
3 ≤ Ysd <10
10 ≤ YsD†
10 ≤ Ysd
[1975-2024]

Figure 6

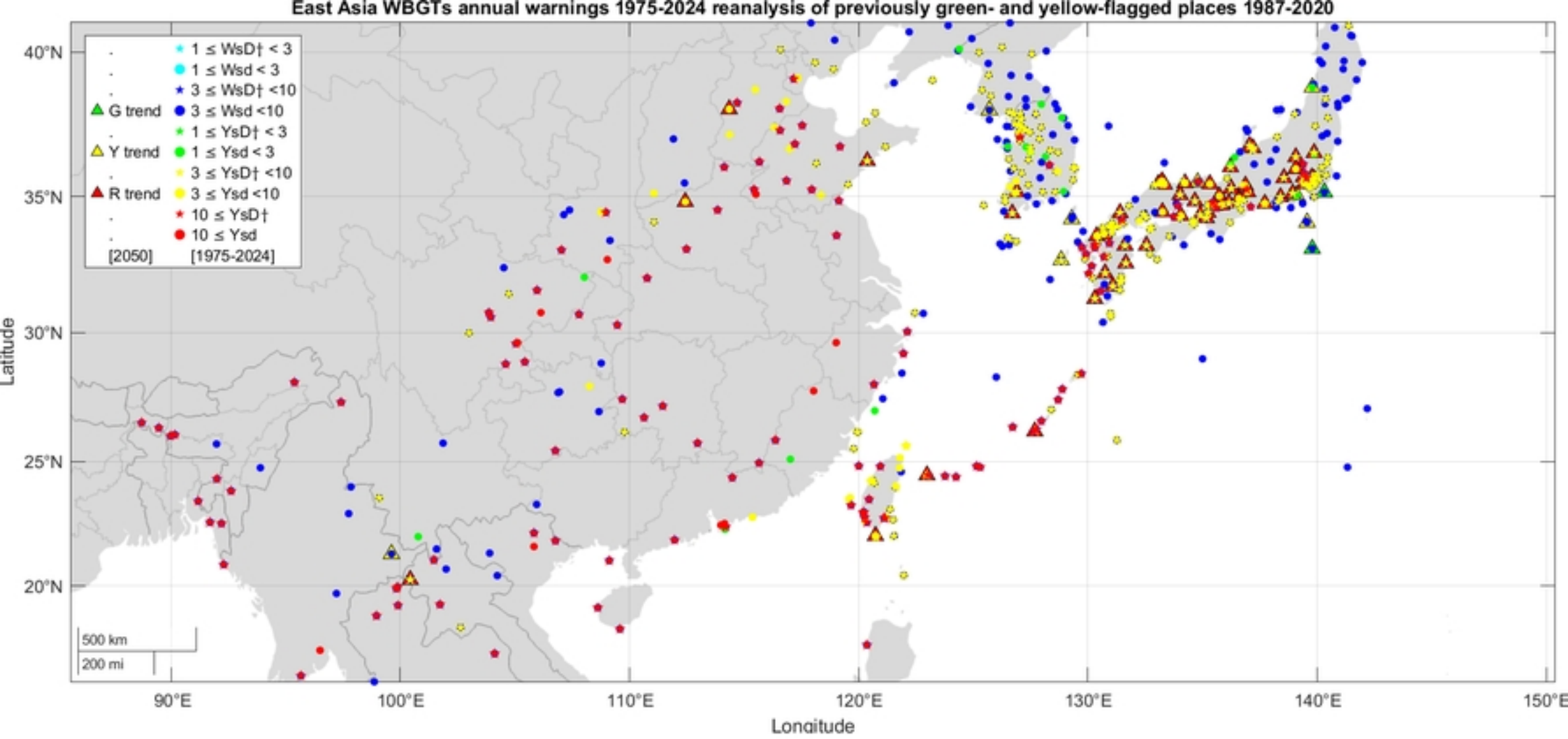
East Asia WBGTs annual warnings 1975-2024 reanalysis of previously green- and yellow-flagged places 1987-2020
1 ≤ WsD† < 3
1 ≤ Wsd < 3
3 ≤ WsD† <10
G trend
3 ≤ Wsd <10
1 ≤ YsD† < 3
Y trend
1 ≤ Ysd < 3
3 ≤ YsD† <10
R trend
3 ≤ Ysd <10
10 ≤ YsD†
10 ≤ Ysd
[2050]
[1975-2024]
40°N
35°N
30°N
25°N
20°N
Latitude
500 km
200 mi
90°E
100°E
110°E
120°E
130°E
140°E
150°E
Longitude

Figure 7

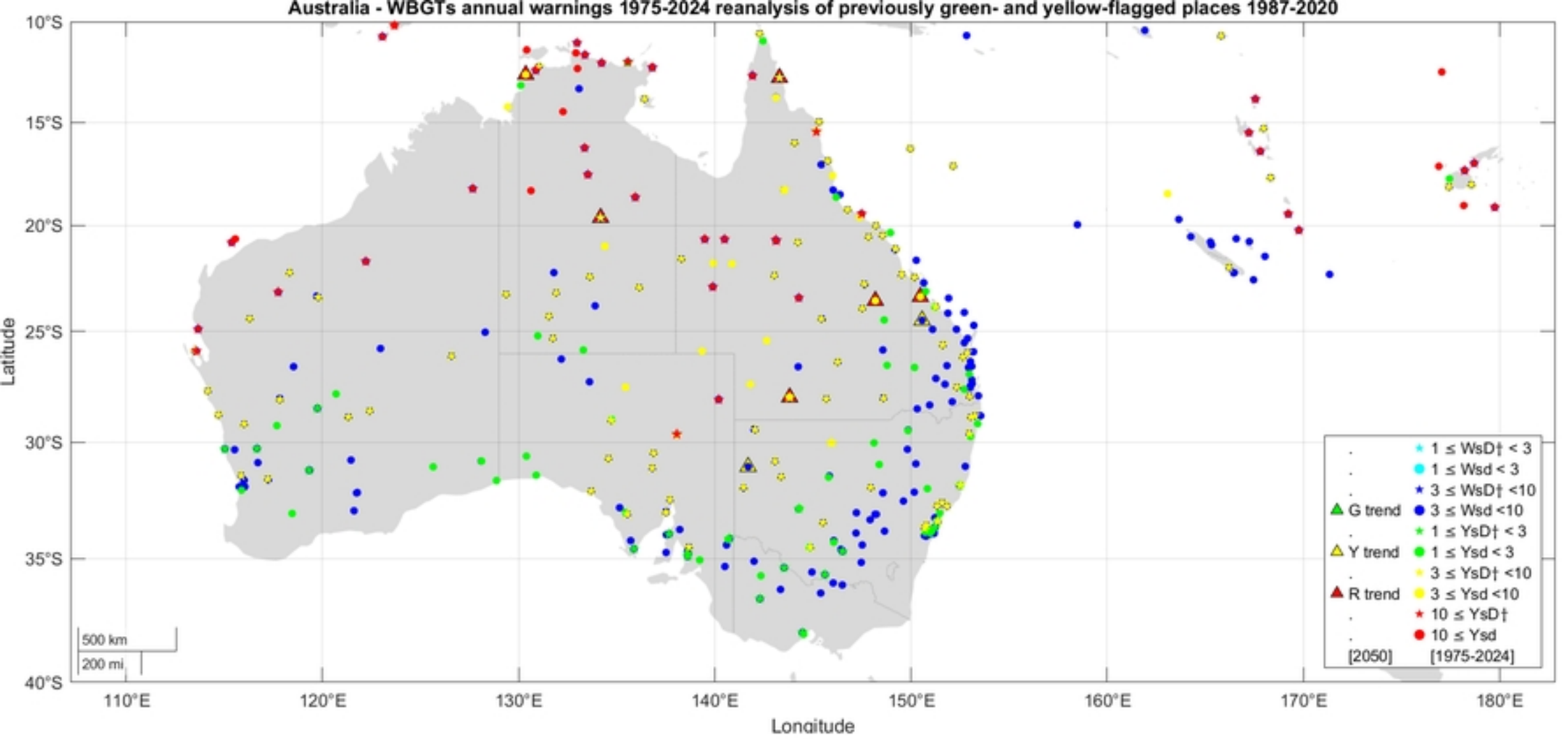
Australia - WBGTs annual warnings 1975-2024 reanalysis of previously green- and yellow-flagged places 1987-2020
10°S
15°S
20°S
25°S
30°S
35°S
40°S
Latitude
110°E
120°E
130°E
140°E
150°E
160°E
170°E
180°E
Longitude
500 km
200 mi
G trend
Y trend
R trend
[2050]
1 ≤ WsD† < 3
1 ≤ Wsd < 3
3 ≤ WsD† <10
3 ≤ Wsd <10
1 ≤ YsD† < 3
1 ≤ Ysd < 3
3 ≤ YsD† <10
3 ≤ Ysd <10
10 ≤ YsD†
10 ≤ Ysd
[1975-2024]

Figure 8